Diagnosing Conditions in Proton Beam-Heated Plasmas Using Fluorine K_α Emission and Absorption Spectra

J.J. MacFarlane and P. Wang

July 1993

UWFDM-917

FUSION TECHNOLOGY INSTITUTE

UNIVERSITY OF WISCONSIN

MADISON WISCONSIN

Diagnosing Conditions in Proton Beam-Heated Plasmas Using Fluorine K_α Emission and Absorption Spectra

J. J. MacFarlane and P. Wang

Fusion Technology Institute
University of Wisconsin-Madison
1500 Johnson Drive
Madison, WI 53706

July 1993

UWFDM-917

1. Introduction

K_α emission and absorption spectroscopy [1-7] can be used to diagnose plasma conditions in targets heated by intense proton beams. In this progress report, we discuss how the K_α line spectrum from a thin fluorine tracer layer could be used to diagnose target plasma conditions in KALIF experiments. This complements K_α studies carried out for other tracers, such as Al [8-11], Mg [12], and O [13]. Below, we discuss several issues relevant to KALIF temperature diagnostic experiments, including: optimal tracer and tamper thicknesses, detector sensitivity and spectral resolution, and expected temperature and density dependencies for K_α and K_β absorption and emission spectra.

In the calculations below, we examine fluorine (F) as the tracer material. This was chosen for several reasons. Firstly, any material with $Z \leq 10$ will provide good temperature sensitivity at low plasma temperatures ($T \sim 2-20$ eV) because the K_α satellites are noticeably blue-shifted even for the lowest ionization stages. This is due to the fact that electrons are immediately stripped from the L-shell as the tracer layer becomes ionized. Thus, for initial KALIF experiments, in which a relatively low power density beam would be produced with a B_θ diode, a tracer which provides good temperature sensitivity at $T \lesssim 20$ eV is important. Second, F K_α lines occur at $\lambda \sim 17-18.5$ Å. At longer wavelengths — which occur for lower-Z materials — it becomes more difficult to obtain good spectral measurements [14,15]. The F K_α wavelengths are also reasonably nearby other potentially good tracer materials — such as Na ($\lambda \approx 11-12$ Å), Mg ($\lambda \approx 9-10$ Å), and Al ($\lambda \approx 7.5-8.5$) — which could also be used in higher-temperature experiments with the applied-B diode on KALIF. Third, it should be possible to manufacture a target with a thin F tracer [15]. In addition, if a tracer is made with NaF or MgF compounds, which can easily be produced in thin layers [15], one could simultaneously observe the K_α spectrum from 2 elements, thereby providing additional diagnostic constraints. (It is currently envisioned that in a future series of PBFA-II experiments at Sandia National Laboratories similar measurements will be made simultaneously of Mg and Al tracers.)

In the calculations discussed below, the conditions for the F-tracer were varied as follows:

$$2 \lesssim T \leq 20 \text{ eV} \qquad \text{(tracer temperature)}$$

$$10^{18}\,\text{cm}^{-3} \leq n \leq 10^{22}\,\text{cm}^{-3} \qquad \text{(tracer ion density)}$$

$$10\,\text{Å} \lesssim L_o \lesssim 100\,\mu\text{m} \qquad \text{(original tracer thickness)} \quad .$$

In our atomic models for fluorine a total of 271 energy levels were considered, which were distributed over all 10 ionization stages. Roughly 125 of these were autoionizing levels, of which 50-60 had M-shell electrons. Thus, several K_α lines with M-shell spectator electrons and several K_β lines appear in the computed spectra. Because of the possibility of measuring both emission and absorption spectra, results are presented for both.

In each calculation we assumed a 1 MeV proton beam with a 0.3 TW/cm^2 power density. This corresponds roughly to the parameters for KALIF using the B_θ diode. The computed intensities are somewhat sensitive to the beam energy (proton velocity). A beam energy of 1 MeV corresponds to just below the peak in the proton impact ionization cross section curve (see Fig. 1). The line intensities are proportional to the cross section. In addition, the line intensities are also proportional to the beam current density (neglecting, of course, effects of beam current density on the plasma temperature).

2. Optimal Target Thickness

For K_α emission spectral observations, one would like the diagnostic tracer to be as thin as possible (to mitigate opacity effects in the observed spectrum), while still having enough signal to detect. The minimum thickness depends on: (1) the material properties of the tracer and the ability to manufacture it, and (2) the sensitivity of the detector — i.e., the signal-to-noise — which requires knowledge of both the detector properties and possible presence of external x-ray sources, "UV leaks", etc. We have calculated the strength of the signal — i.e., the K_α line flux — as a function of the F tracer layer thickness. This is shown in Fig. 2, where the K_α flux between 0.4 and 1.1 keV is plotted as a function of tracer solid density thickness (L_o) for a F plasma at $T = 10$ eV and $n = 6 \times 10^{20}$ cm^{-3}. (It was assumed this density corresponds to 1% of solid density (n_o); however, n_o depends of course on the fluorine compound chosen.) The density conditions are similar to those occurring in recent light ion beam experiments at Sandia National Laboratories, in which the planar target expands $\sim 10^2 - 10^3$ times while the beam irradiates the target. Note that the *plasma* thickness in each calculation was 100 times the stated solid density thickness, so that $nL = n_o L_o$.

Figure 2 shows that the flux is approximately proportional to the tracer thickness for $L_o < 10^3$ Å. For $L_o \gtrsim 10^3$ Å, the K_α lines become optically thick. Note that as the tracer thickness exceeds 10 μm, the flux becomes constant. This occurs because the plasma becomes optically thick throughout this spectral region. Thus, increasing the tracer thickness beyond 10 μm will not produce significantly more photons at the detector.

Because opacity effects can lead to difficulties in interpreting spectra, it is recommended that the tracer thickness be kept to $\lesssim 1\,\mu$m if possible.

If absorption spectral measurements are to be made, the optimum tracer thickness is $\approx 10^3$ Å (see, e.g., Perry et al. 1991; see also Figures 6-10). This is because the K_α line optical depths are $\sim 10^0 - 10^1$ at this thickness.

The flux at the detector can be estimated as follows. Assuming the distance between the target and detector, D, is small compared to the "spot size", the flux at the detector is roughly:

$$\mathcal{F}\,(\text{detector}) = \mathcal{F}\,(\text{calculated}) \cdot \frac{\text{spot area}}{2\pi D^2}\,,$$

where the 2π assumes the photons are distributed more-or-less uniformly over one hemisphere. For $D \approx 10^2$ cm and a spot size of about 1 cm^2, a typical flux at the detector would be:

$$\begin{aligned}\mathcal{F}\,(\text{detector}) &\simeq (10^{11}\,\text{erg/cm}^2\text{/s/eV})\,\frac{(1\,\text{cm}^2)}{(2\pi)(100\,\text{cm})^2} \\ &\simeq 1.6\times 10^6\,\text{erg/cm}^2\text{/s/eV}\,.\end{aligned}$$

For 700 eV photons, this corresponds to about

$$\text{F} \quad (\text{detector}) \simeq 1\times 10^{15}\ \text{photons/cm}^2\text{/s/spectral ``bin''}$$

for a spectral resolution of 10^3.

3. Spectral Resolution

In regards to spectral resolution, a resolution of $\lambda/\Delta\lambda$ of $\gtrsim 10^3$ will easily resolve the "major satellite features" — i.e., each ionization stage. In recent PBFA-II experiments [7], a spectrometer with $\lambda/\Delta\lambda$ of $\sim 1200 - 1500$ was used. At this resolution the structure within the major satellite features begins to be resolved. In laser-produced plasma experiments at Lawrence Livermore National Laboratory [6] detailed structure within the major satellite features was clearly seen using a spectral resolution of about 2500. The measured absorption spectra were reproduced quite well in calculations by Abdallah et al. [16], and more recently by us [13]. The ability to simulate the LLNL measurements in detail suggests that reliable determinations of plasma conditions can be made using the K_α technique.

Figure 3 shows calculated K_α emission and absorption satellite spectra for F at $T = 10$ eV, $n = 1 \times 10^{20}$ cm^{-3}, and $L_o = 1000$ Å. The dashed vertical lines correspond to a spectral resolution of $\lambda/\Delta\lambda = 1000$. The K_α lines for each ionization stage of F correspond roughly to the following wavelength regions:

Ion	Wavelength (Å)
He_α	16.82
Li-like	17.1 - 17.2
Be-like	17.3 - 17.4
B-like	17.5 - 17.7
C-like	17.7 - 17.9
N-like	18.0 - 18.1
O-like	18.1 - 18.2

Note that for resolutions greater than 1000, individual K_α lines begin to be resolved. This raises the possibility of using K_α line intensity ratios to diagnose both temperatures and densities. We have recently begun to study this for He-like and Li-like K_α lines of Mg and Al tracers for Sandia National Laboratories [12]. It thus appears that *significantly greater constraints on plasma temperatures and densities may be achieved if several prominent K_α lines can be individually resolved.* This of course assumes that the spectral measurement would be time-resolved as well.

4. Possible Target Designs

Based on the above considerations, as well as conversations with KfK and Sandia personnel, we next sketch out one possible experimental arrangement for measuring the temperature in a proton beam-heated plasma. Figure 4 shows a "plastic sandwich" target composed of a $0.1 - 1\,\mu$m-thick NaF tracer sandwiched between two $1 - 2\,\mu$m-thick plastic tampers. The tampers are used to keep the density in the tracer layer approximately uniform.

The attenuation of x-ray photons by the tamper in the F K_α spectral region can potentially be significant and must be considered in the target design. This is true both for K_α *emission* from the tracer layer and for the absorption of x-ray backlighter photons in an absorption experiment. The carbon K-shell photoioinization cross section at 18 Å is about 0.12 Mb. Assuming a density of 4×10^{22} C atoms/cm^3 in the plastic tampers, the absorption coefficient is:

$$\kappa(\lambda = 18\,\mathring{A}) = 0.5\,\mu\mathrm{m}^{-1}\,.$$

Thus, 18 Å photons will be attenuated about 40% ($\exp(-\kappa L)$) for each micron of plastic tamper. Greater attenuation occurs along lines-of-sight not perpendicular to the target surface. Hydrodynamics calculations could be performed to predict the evolution of the tracer and tamper regions.

Al could be used as an alternative to using CH_2 tampers. The cross section for photoabsorption of 18 Å photons for Al is about 0.15 Mb; i.e., only about 25% higher than that for C. Considering a NaF tracer, the cross sections at the K_α wavelengths of Na are lower for both CH_2 and Al tampers. Thus, tamper photoabsorption of the F K_α photons will provide greater constraints for the tamper thicknesses.

5. Dependence of F K_α Spectra on Tracer Thickness

Figures 5(a) - 5(d) show how the K_α spectra are predicted to vary as a function of the tracer thickness. In each case the absorption spectrum, which could be observed if an x-ray backlighter is used, is plotted on the top. The corresponding emission spectrum is shown on the bottom. Note that the scales for both the x- and y-axes are not the same in all figures! Note also that the spectra have not been corrected for instrumental broadening, which is unknown at this time.

From the absorption spectra, it is clear that tracers much thicker than 1 μm produce far too much absorption. The 10 μm case (Fig. 5(d)) shows that most of the backlighter photons will be absorbed by the tracer before reaching the detector. In addition, the emission spectrum starts to become skewed to apparent higher ionization stage. That is, the intensities of lines from less abundant ions increase as the thickness increases, but those from the relatively abundant ions do not because of opacity effects. **This again points out the need to keep tracer thicknesses to $\lesssim 1\,\mu$m.**

6. Dependence of F K_α Spectra on Temperature and Density

Figures 6-10 show how the calculated absorption and emission spectra vary with temperature and density. For each figure, plots (a), (b), (c), and (d) show results for plasma temperatures of 2, 5, 10, and 20 eV, respectively. Lines are identified for the $n = 10^{20}\,\mathrm{cm}^{-3}$ series (Fig. 6(a)-(d)), and also in Table 1. Table 1 shows the upper and lower states of each K_α and K_β transition considered, its ionization stage, transition energy, wavelength, and fluorescence yield.

To examine the temperature dependence, we focus our attention on the $n = 10^{20}\,\mathrm{cm}^{-3}$ series (this corresponds roughly to the density at which the maximum plasma temperature was attained in the PBFA-II Al K_α experiments). The results are shown in Fig. 6. At $T = 2$ eV, both absorption and emission K_α lines from O-like fluorine ($\lambda \simeq 18.2$ Å) are seen. K_β (a $3p \rightarrow 1s$) transition from O-like F ($\lambda = 17.4$ Å) is seen in absorption, but is extremely weak in emission. This results from the fact that the absorption is a reflection of the lower state population of the transition (of the type $1s^2\,2s^2\,2p^4$), while the emission is proportional to the population of the upper state (for O-like K_β, this is $1s^1\,2s^2\,2p^4\,3p^1$, which is produced by thermal excitation of FI, followed by a proton impact ionization). Also seen in emission is N-like F K_α ($\lambda \simeq 18.0$ Å). [Note that F-like K_α and K_β should also be seen in absorption, but were not included in the present atomic models.]

As the tracer is heated to $T = 5$ eV, both K_α and K_β from N-like F are seen in absorption while C- and B-like F appear in emission. At $T = 10$ eV, C- and B-like F are seen in absorption, while B-, Be-, and Li-like F are seen in emission. Note that the strongest He-like resonance line ($1s^1\,2p^1\,{}^1P \rightarrow 1s^2\,{}^1S$) ($\lambda = 16.8$ Å) begins to appear at this temperature. The upper state of this transition is of course not an autoionizing level, and therefore has a fluorescence yield of 1. Because of this, the intensity of this line can be significantly stronger than the K_α lines from the lower ionization stages, which typically have fluorescence yields of $\sim 10^{-2}$. Figure 6(d) shows the results for $T = 20$ eV. At this temperature the He-like and Li-like lines dominate the emission spectrum. Note that the intensity of the He-like line is almost 2 orders of magnitude higher than the K_α intensities at the lower temperatures. It is thought that measuring the intensity ratios of individual K-shell lines from He-like and Li-like tracer ions may provide accurate determinations of plasma temperatures and densities [12]. However, more work needs to be done in this area to confirm this.

Acknowledgements

The authors thank B. Goel and A. Ludmirsky of KfK and J. Bailey of Sandia National Laboratories for valuable discussions. This work has been supported by Kernforschungszentrum Karlsruhe through Fusion Power Associates.

References

1. A. Hauer, R. D. Cowan, B. Yaakobi, O. Barnouin, and R. Epstein, *Phys. Rev.* **A 34**, 411 (1986).

2. C. Chenais-Popovics, C. Fievet, J. P. Geindre, J. C. Gauthier, E. Luc-Koenig, J. F. Wyart, H. Pepin, and M. Chaker, *Phys. Rev.* **A 40**, 3194 (1989).

3. J. Bruneau, C. Chenais-Popovics, D. Desenne, J.-C. Gauthier, J.-P. Geindre, M. Klapisch, J.-P. Le Breton, M. Louis-Jacquet, D. Naccache, and J.-P. Perrine, *Phys. Rev. Lett.* **65**, 1435 (1990).

4. S. J. Davidson, J. M. Foster, C. C. Smith, K. A. Warburton, and S. J. Rose, *Appl. Phys. Lett.* **52**, 847 (1988).

5. D. M. O'Neil, C. L. S. Lewis, D. Neely, and S. J. Davidson, *Phys. Rev.* **A 44**, 2641 (1991).

6. T. S. Perry, S. J. Davidson, F. J. D. Serduke, D. R. Bach, C. C. Smith, J. M. Foster, R. J. Doyas, R. A. Ward, C. A. Iglesias, F. J. Rogers, J. Abdallah, Jr., R. E. Stewart, J. D. Kilkenny, and R. W. Lee, *Phys. Rev. Lett.* **67**, 3784 (1991).

7. J. Bailey, A. L. Carlson, G. Chandler, M. S. Derzon, R. J. Dukart, B. A. Hammel, D. J. Johnson, T. R. Lockner, J. Maenchen, E. J. McGuire, T. A. Mehlhorn, W. E. Nelson, L. E. Ruggles, W. A. Stygar, and D. F. Wenger, *Lasers and Particle Beams* **8**, 555 (1990).

8. J. J. MacFarlane, P. Wang, J. Bailey, T. A. Mehlhorn, R. J. Dukart, and R. C. Mancini, *Phys. Rev.* **E 47**, 2748 (1993).

9. P. Wang, J. J. MacFarlane, and G.A. Moses, *Phys. Rev.* **E**, in press (1993).

10. J. J. MacFarlane, P. Wang, T. A. Mehlhorn, J. Bailey, and R. J. Dukart, *Rev. Sci. Instrum.* **63**, 5062 (1992).

11. J. J. MacFarlane and P. Wang, *Lasers Particle Beams* **10**, 349 (1992).

12. J. J. MacFarlane and P. Wang, "Theoretical Spectral Diagnostic Analyses in Support of PBFA-II Beam-Plasma Interaction Experiments," University of Wisconsin Fusion Technology Institute Report UWFDM-913 (1993).

13. J. J. MacFarlane, P. Wang, D. L. Henderson, and O. Yasar, "Numerical Simulations of High Energy Density Plasmas in Support of KALIF Experiments," Fusion Power Associates Report FPA-93-1 (1993).

14. B. Goel and A. Ludmirsky, personal communication (1993).

15. J. Bailey, personal communication (1993).

16. J. Abdallah, Jr., R. E. H. Clark, and J. M. Peek, Phys. Rev. **A 44**, 4072 (1991).

Table 1. Fluorine K_α and K_β Lines

Upper Level		Lower Level		Iz. Stage	Energy	Wave-length	Fl. Yield
1s(1)2s(2)2p(5)	1P	1s(2)2s(2)2p(4)	1S	2	679.99	18.233	.022
1s(1)2s(1)2p(5)	2P	1s(2)2s(1)2p(4)	2P	3	680.36	18.223	.022
1s(1)2s(2)2p(5)	3P	1s(2)2s(2)2p(4)	3P	2	681.57	18.190	.010
1s(1)2s(2)2p(5)	1P	1s(2)2s(2)2p(4)	1D	2	682.21	18.173	.022
1s(1)2s(1)2p(6)	3S	1s(2)2s(1)2p(5)	3P	2	683.17	18.148	.021
1s(1)2s(1)2p(4)	3P	1s(2)2s(1)2p(3)	3S	4	683.26	18.145	.029
1s(1)2s(1)2p(5)	2P	1s(2)2s(1)2p(4)	2S	3	683.34	18.143	.022
1s(1)2s(2)2p(4)3p(1)	3P	1s(2)2s(2)2p(3)3p(1)	1P	2	683.53	18.138	.015
1s(1)2s(2)2p(4)3p(1)	3P	1s(2)2s(2)2p(3)3p(1)	3D	2	683.54	18.138	.015
1s(1)2s(2)2p(4)3s(1)	3D	1s(2)2s(2)2p(3)3s(1)	3P	2	684.63	18.109	.012
1s(1)2s(2)2p(4)	2D	1s(2)2s(2)2p(3)	2P	3	686.17	18.068	.012
1s(1)2s(2)2p(4)3p(1)	3D	1s(2)2s(2)2p(3)3p(1)	3P	2	686.20	18.068	.012
1s(1)2s(2)2p(4)3p(1)	5P	1s(2)2s(2)2p(3)3p(1)	5P	2	686.31	18.065	.007
1s(1)2s(2)2p(4)3p(1)	3S	1s(2)2s(2)2p(3)3p(1)	3P	2	686.39	18.063	.032
1s(1)2s(1)2p(5)	2P 2	1s(2)2s(1)2p(4)	2P	3	686.43	18.062	.022
1s(1)2s(2)2p(4)3s(1)	5P	1s(2)2s(2)2p(3)3s(1)	5S	2	686.46	18.061	.007
1s(1)2s(2)2p(4)3s(1)	3P	1s(2)2s(2)2p(3)3s(1)	3S	2	686.50	18.060	.031
1s(1)2s(2)2p(4)	2P	1s(2)2s(2)2p(3)	2P	3	686.57	18.058	.032
1s(1)2s(2)2p(4)3p(1)	5D	1s(2)2s(2)2p(3)3p(1)	5P	2	686.58	18.058	.007
1s(1)2s(2)2p(4)3p(1)	3P	1s(2)2s(2)2p(3)3p(1)	3P	2	686.81	18.051	.015
1s(1)2s(2)2p(4)3p(1)	5S	1s(2)2s(2)2p(3)3p(1)	5P	2	686.98	18.047	.007
1s(1)2s(2)2p(4)	4P	1s(2)2s(2)2p(3)	4S	3	686.99	18.047	.007
1s(1)2s(2)2p(4)3s(1)	3D	1s(2)2s(2)2p(3)3s(1)	3D	2	687.28	18.039	.012
1s(1)2s(1)2p(5)	2P	1s(2)2s(1)2p(4)	2D	3	687.47	18.034	.022
1s(1)2s(2)2p(4)	2D	1s(2)2s(2)2p(3)	2D	3	687.82	18.025	.012
1s(1)2s(1)2p(5)	4P	1s(2)2s(1)2p(4)	4P	3	688.18	18.016	.018
1s(1)2s(2)2p(4)	2P	1s(2)2s(2)2p(3)	2D	3	688.22	18.015	.032
1s(1)2s(1)2p(4)	1D	1s(2)2s(1)2p(3)	1P	4	688.87	17.998	.020
1s(1)2s(2)2p(4)	2S	1s(2)2s(2)2p(3)	2P	3	688.98	17.995	.014
1s(1)2s(1)2p(5)	2P 2	1s(2)2s(1)2p(4)	2S	3	689.40	17.984	.022
1s(1)2p(5)	1P	1s(2)2p(4)	1S	4	690.42	17.957	.037
1s(1)2s(1)2p(4)	3P	1s(2)2s(1)2p(3)	3P	4	691.45	17.930	.029
1s(1)2s(1)2p(4)	1D	1s(2)2s(1)2p(3)	1D	4	691.91	17.918	.020
1s(1)2s(2)2p(3)3s(1)	4D	1s(2)2s(2)2p(2)3s(1)	4P	3	692.56	17.902	.008
1s(1)2s(1)2p(4)	3D	1s(2)2s(1)2p(3)	3P	4	692.64	17.900	.022
1s(1)2s(1)2p(4)	3P 2	1s(2)2s(1)2p(3)	3S	4	693.21	17.885	.029
1s(1)2s(2)2p(3)3s(1)	2S	1s(2)2s(2)2p(2)3s(1)	2P	3	693.38	17.880	.064
1s(1)2s(2)2p(3)3s(1)	4S 2	1s(2)2s(2)2p(2)3s(1)	4P	3	693.45	17.879	.063
1s(1)2s(1)2p(5)	2P 2	1s(2)2s(1)2p(4)	2D	3	693.53	17.877	.022
1s(1)2s(1)2p(4)	1P	1s(2)2s(1)2p(3)	1P	4	693.75	17.871	.069
1s(1)2s(1)2p(4)	1S	1s(2)2s(1)2p(3)	1P	4	693.83	17.869	.026
1s(1)2s(2)2p(3)	3D	1s(2)2s(2)2p(2)	3P	4	694.17	17.860	.008

Table 1 (Continued)

Upper Level		Lower Level		Iz. Stage	Energy	Wave-length	Fl. Yield
1s(1)2s(1)2p(3)	2D	1s(2)2s(1)2p(2)	2P	5	694.32	17.856	.023
1s(1)2s(2)2p(3)	1P	1s(2)2s(2)2p(2)	1S	4	694.37	17.855	.030
1s(1)2s(1)2p(4)	3P	1s(2)2s(1)2p(3)	3D	4	694.49	17.852	.029
1s(1)2s(1)2p(4)	5P	1s(2)2s(1)2p(3)	5S	4	694.73	17.846	.016
1s(1)2s(2)2p(3)	3S	1s(2)2s(2)2p(2)	3P	4	695.07	17.837	.066
1s(1)2s(2)2p(3)	1D	1s(2)2s(2)2p(2)	1D	4	695.20	17.834	.026
1s(1)2p(5)	3P	1s(2)2p(4)	3P	4	695.42	17.828	.018
1s(1)2s(1)2p(4)	3D	1s(2)2s(1)2p(3)	3D	4	695.67	17.822	.022
1s(1)2s(2)2p(2)3p(1)	3D	1s(2)2s(2)2p(1)3p(1)	3P	4	695.94	17.815	.010
1s(1)2s(2)2p(3)	3P	1s(2)2s(2)2p(2)	3P	4	696.09	17.811	.009
1s(1)2p(5)	1P	1s(2)2p(4)	1D	4	696.56	17.799	.037
1s(1)2s(1)2p(4)	1P	1s(2)2s(1)2p(3)	1D	4	696.79	17.793	.069
1s(1)2s(2)2p(3)	1P	1s(2)2s(2)2p(2)	1D	4	697.12	17.785	.030
1s(1)2s(1)2p(4)	3S	1s(2)2s(1)2p(3)	3P	4	697.57	17.773	.028
1s(1)2s(1)2p(3)	2P	1s(2)2s(1)2p(2)	2P	5	697.88	17.765	.031
1s(1)2p(4)	2D	1s(2)2p(3)	2P	5	699.63	17.721	.021
1s(1)2s(1)2p(3)	2D 2	1s(2)2s(1)2p(2)	2P	5	700.39	17.702	.023
1s(1)2p(4)	2P	1s(2)2p(3)	2P	5	700.39	17.701	.064
1s(1)2s(1)2p(3)	2P	1s(2)2s(1)2p(2)	2S	5	700.65	17.695	.031
1s(1)2s(1)2p(3)	4S	1s(2)2s(1)2p(2)	4P	5	701.77	17.667	.136
1s(1)2s(2)2p(2)3s(1)	3D	1s(2)2s(2)2p(1)3s(1)	3P	4	701.78	17.666	.010
1s(1)2s(1)2p(3)	2D	1s(2)2s(1)2p(2)	2D	5	702.07	17.659	.023
1s(1)2s(1)2p(3)	4D	1s(2)2s(1)2p(2)	4P	5	702.31	17.653	.017
1s(1)2s(2)2p(2)3s(1)	3P 2	1s(2)2s(2)2p(1)3s(1)	3P	4	702.66	17.644	.082
1s(1)2p(4)	4P	1s(2)2p(3)	4S	5	702.73	17.643	.016
1s(1)2s(2)2p(2)	2D	1s(2)2s(2)2p(1)	2P	5	703.60	17.621	.010
1s(1)2s(1)2p(3)	2P 2	1s(2)2s(1)2p(2)	2P	5	703.95	17.612	.031
1s(1)2p(4)	2D	1s(2)2p(3)	2D	5	704.09	17.609	.021
1s(1)2s(1)2p(3)	2S	1s(2)2s(1)2p(2)	2P	5	704.31	17.603	.745
1s(1)2s(2)2p(2)	2P	1s(2)2s(2)2p(1)	2P	5	704.46	17.599	.060
1s(1)2p(4)	2P	1s(2)2p(3)	2D	5	704.85	17.590	.064
1s(1)2s(1)2p(3)	2P	1s(2)2s(1)2p(2)	2D	5	705.63	17.570	.031
1s(1)2s(1)2p(3)	4P	1s(2)2s(1)2p(2)	4P	5	705.86	17.564	.024
1s(1)2s(2)2p(2)	2S	1s(2)2s(2)2p(1)	2P	5	706.63	17.545	.013
1s(1)2s(1)2p(3)	2P 2	1s(2)2s(1)2p(2)	2S	5	706.72	17.543	.031
1s(1)2p(4)	2S	1s(2)2p(3)	2P	5	707.19	17.531	.028
1s(1)2s(2)2p(1)3p(1)	2P	1s(2)2s(2)3p(1)	2P	5	707.38	17.527	.055
1s(1)2s(1)2p(3)	2D 2	1s(2)2s(1)2p(2)	2D	5	708.15	17.508	.023
1s(1)2s(2)2p(1)3p(1)	2D	1s(2)2s(2)3p(1)	2P	5	709.54	17.473	.050
1s(1)2s(1)2p(2)	1D	1s(2)2s(1)2p(1)	1P	6	709.63	17.471	.020
1s(1)2p(3)	1P	1s(2)2p(2)	1S	6	709.86	17.465	.068
1s(1)2p(3)	3D	1s(2)2p(2)	3P	6	710.33	17.454	.018
1s(1)2s(2)2p(1)3p(1)	2S	1s(2)2s(2)3p(1)	2P	5	710.60	17.447	.053

Table 1 (Continued)

Upper Level		Lower Level		Iz. Stage	Energy	Wave-length	Fl. Yield
1s(1)2s(2)2p(4)3p(1)	3D	1s(2)2s(2)2p(4)	3P	2	711.66	17.421	.012
1s(1)2s(1)2p(3)	2P 2	1s(2)2s(1)2p(2)	2D	5	711.71	17.420	.031
1s(1)2s(2)2p(4)3p(1)	3S	1s(2)2s(2)2p(4)	3P	2	711.86	17.416	.032
1s(1)2p(3)	1D	1s(2)2p(2)	1D	6	711.95	17.414	.051
1s(1)2p(3)	3S	1s(2)2p(2)	3P	6	712.25	17.407	1.000
1s(1)2s(2)2p(4)3p(1)	3P	1s(2)2s(2)2p(4)	3P	2	712.28	17.406	.015
1s(1)2s(1)2p(2)	3P	1s(2)2s(1)2p(1)	3P	6	712.60	17.398	.095
1s(1)2s(2)2p(1)3p(1)	2D 2	1s(2)2s(2)3p(1)	2P	5	713.03	17.388	.050
1s(1)2s(2)2p(1)3s(1)	2P 2	1s(2)2s(2)3s(1)	2S	5	713.20	17.384	.047
1s(1)2s(1)2p(2)	3D	1s(2)2s(1)2p(1)	3P	6	713.27	17.382	.025
1s(1)2s(1)2p(1)3s(1)	3P	1s(2)2s(1)3s(1)	3S	6	714.34	17.356	.086
1s(1)2s(1)2p(2)	1P	1s(2)2s(1)2p(1)	1P	6	714.73	17.346	.806
1s(1)2s(2)2p(1)	1P	1s(2)2s(2)	1S	6	715.13	17.337	.050
1s(1)2s(1)2p(2)	1S	1s(2)2s(1)2p(1)	1P	6	715.32	17.332	.041
1s(1)2p(3)	3P	1s(2)2p(2)	3P	6	716.09	17.314	.025
1s(1)2p(3)	1P	1s(2)2p(2)	1D	6	717.71	17.274	.068
1s(1)2s(1)2p(2)	3S	1s(2)2s(1)2p(1)	3P	6	718.91	17.246	.063
1s(1)2s(1)2p(2)	3P 2	1s(2)2s(1)2p(1)	3P	6	722.33	17.164	.095
1s(1)2p(2)	2D	1s(2)2p(1)	2P	7	722.60	17.157	.025
1s(1)2p(2)	2P	1s(2)2p(1)	2P	7	723.91	17.126	1.000
1s(1)2s(1)2p(1)	2P	1s(2)2s(1)	2S	7	724.87	17.104	.092
1s(1)2p(1)3p(1)	2P	1s(2)3p(1)	2P	7	726.98	17.054	1.000
1s(1)2p(1)3p(1)	2D	1s(2)3p(1)	2P	7	729.92	16.985	.402
1s(1)2s(1)2p(1)	2P 2	1s(2)2s(1)	2S	7	730.25	16.978	.092
1s(1)2s(2)2p(3)3p(1)	4P	1s(2)2s(2)2p(3)	4S	3	730.30	16.977	.009
1s(1)2p(2)	2S	1s(2)2p(1)	2P	7	732.03	16.936	.064
1s(1)2p(1)3s(1)	2P 2	1s(2)3s(1)	2S	7	734.28	16.885	.778
1s(1)2p(1)	1P	1s(2)	1S	8	737.18	16.818	.000
1s(1)2s(2)2p(2)3p(1)	3S	1s(2)2s(2)2p(2)	3P	4	752.95	16.466	.060
1s(1)2s(2)2p(2)3p(1)	3D	1s(2)2s(2)2p(2)	3P	4	754.61	16.430	.010
1s(1)2s(2)2p(2)3p(1)	3P	1s(2)2s(2)2p(2)	3P	4	755.26	16.415	.012
1s(1)2s(2)2p(1)3p(1)	2P	1s(2)2s(2)2p(1)	2P	5	779.83	15.898	.055
1s(1)2s(2)2p(1)3p(1)	4S	1s(2)2s(2)2p(1)	2P	5	780.00	15.895	1.000
1s(1)2s(2)2p(1)3p(1)	2D	1s(2)2s(2)2p(1)	2P	5	781.99	15.854	.050
1s(1)2s(2)2p(1)3p(1)	2S	1s(2)2s(2)2p(1)	2P	5	783.05	15.833	.053
1s(1)2s(2)2p(1)3p(1)	2D 2	1s(2)2s(2)2p(1)	2P	5	785.48	15.784	.050
1s(1)2s(1)2p(1)3p(1)	3P	1s(2)2s(1)2p(1)	3P	6	798.77	15.521	.086
1s(1)2s(1)2p(1)3p(1)	3D	1s(2)2s(1)2p(1)	3P	6	800.81	15.482	.084
1s(1)2s(1)2p(1)3p(1)	3S	1s(2)2s(1)2p(1)	3P	6	802.22	15.455	.084
1s(1)2p(1)3p(1)	2P	1s(2)2p(1)	2P	7	823.26	15.060	1.000
1s(1)2p(1)3p(1)	2D	1s(2)2p(1)	2P	7	826.19	15.006	.402
2s(1)	hy	1s(1)	hy	9	826.55	15.000	1.000
1s(1)3p(1)	1P	1s(2)	1S	8	857.63	14.456	1.000

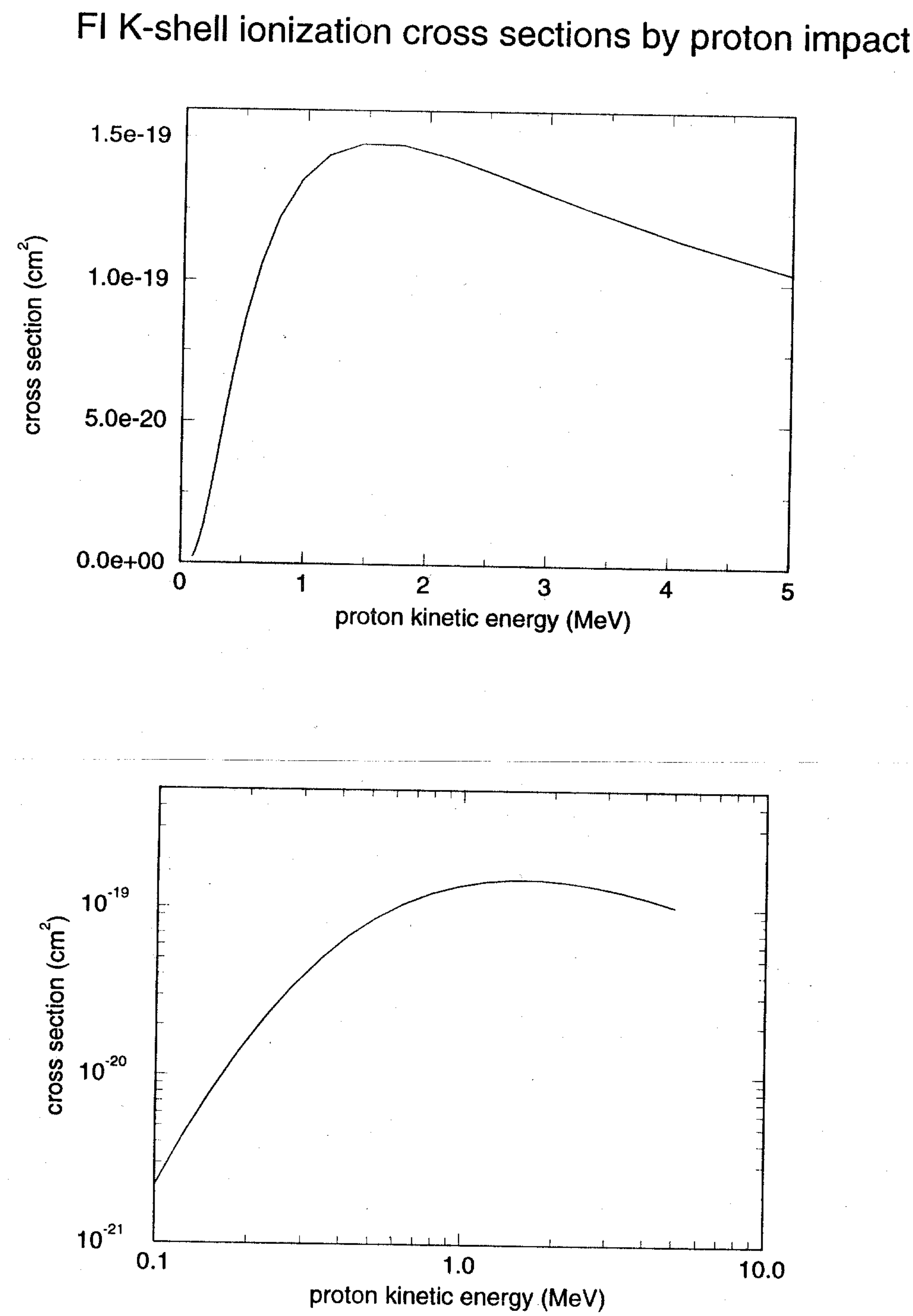

Figure 1. Proton impact ionization cross section for K-shell electrons of neutral F as a function of proton energy.

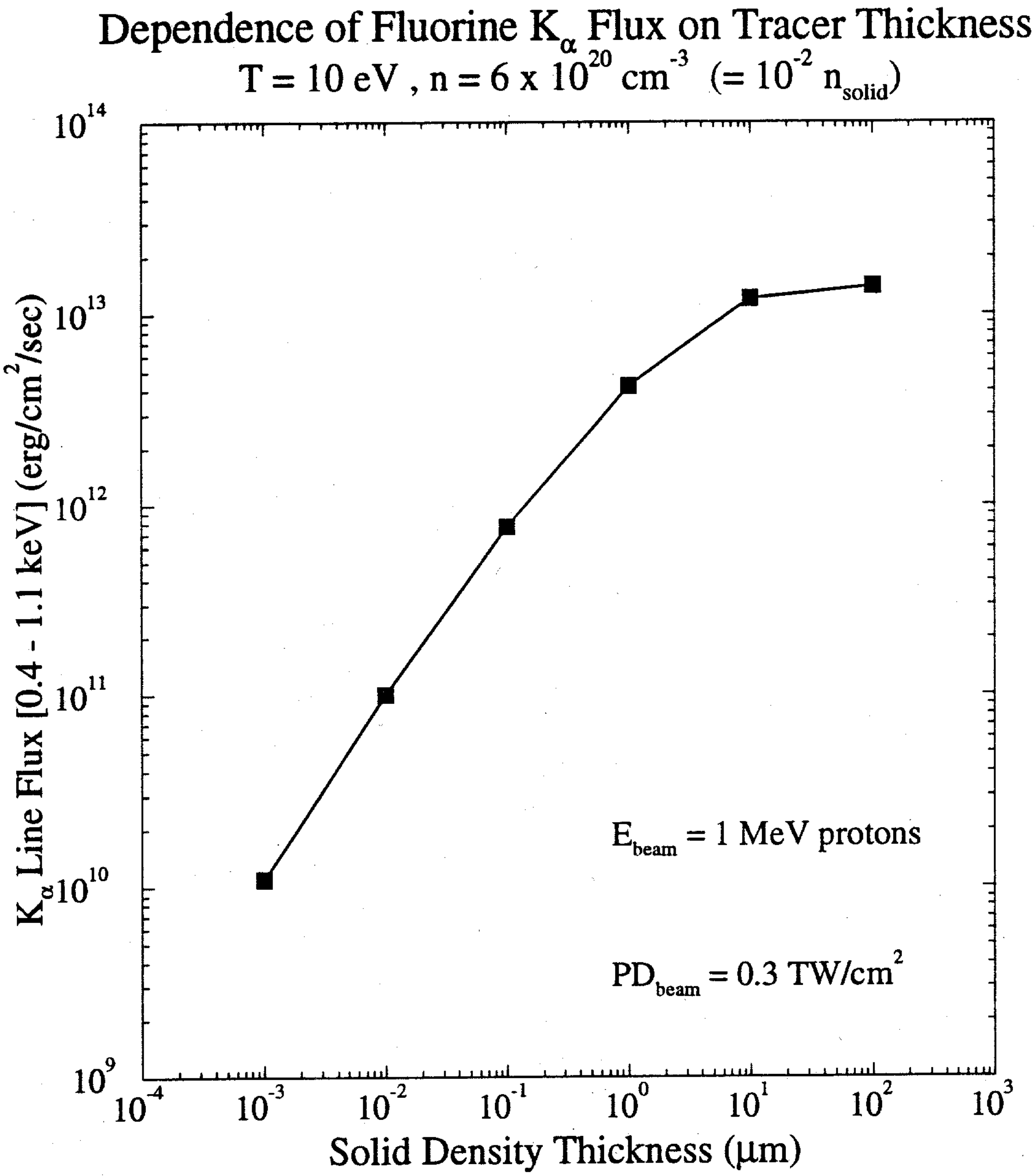

Figure 2. Dependence of F K_α flux between 0.4 and 1.1 keV on tracer solid density thickness for a 1.0 MeV, 0.3 TW/cm^2 proton beam. In each case, the tracer temperature and density are 10 eV and $6 \times 10^{20}\,cm^{-3}$, respectively.

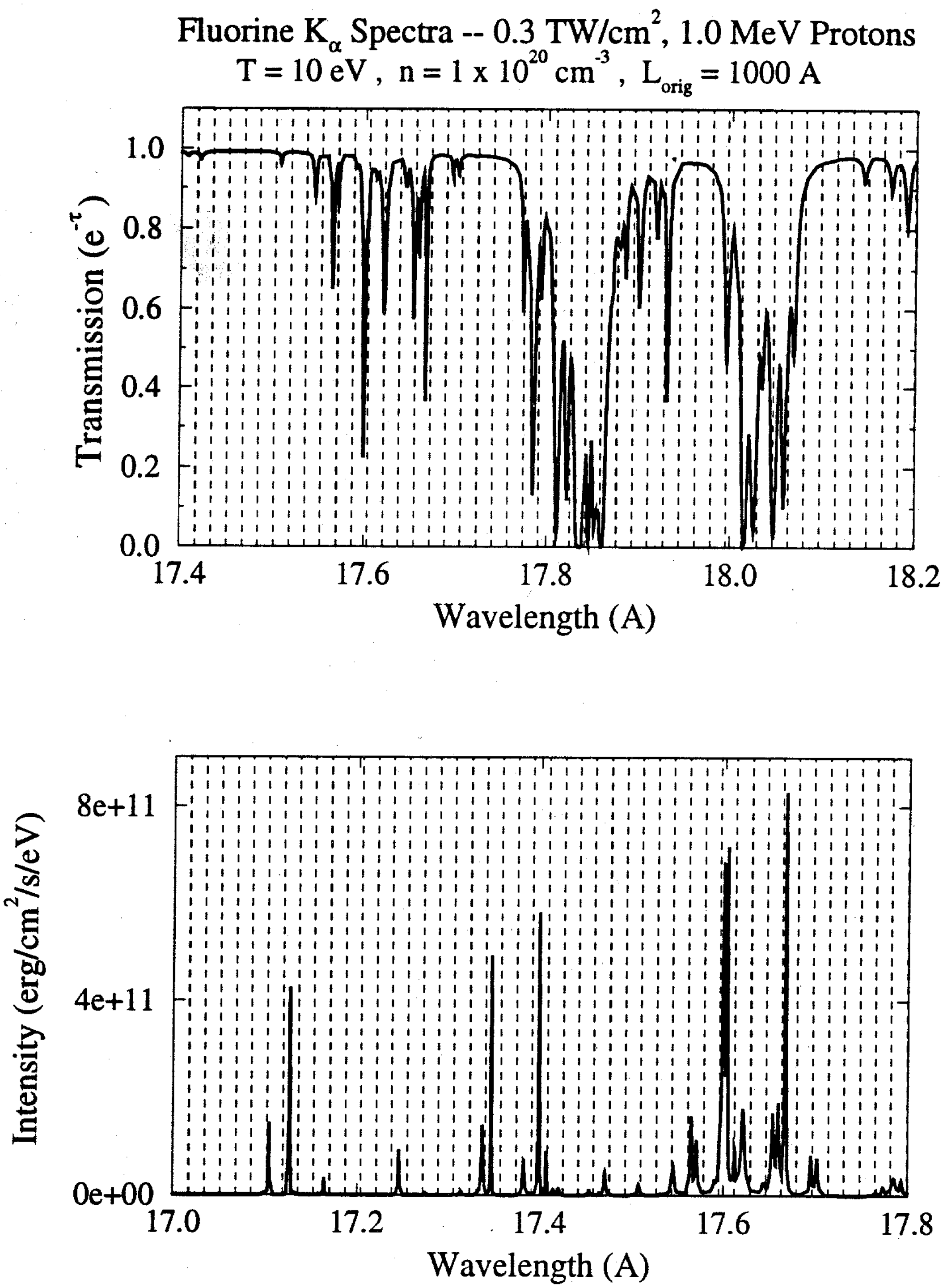

Figure 3. F K_α emission (bottom) and absorption (top) spectra for $T = 10$ eV, $n = 1 \times 10^{20}\,\mathrm{cm}^{-3}$, and $L_o = 1000$ Å. The dashed vertical lines correspond to a spectral resolution of 1000.

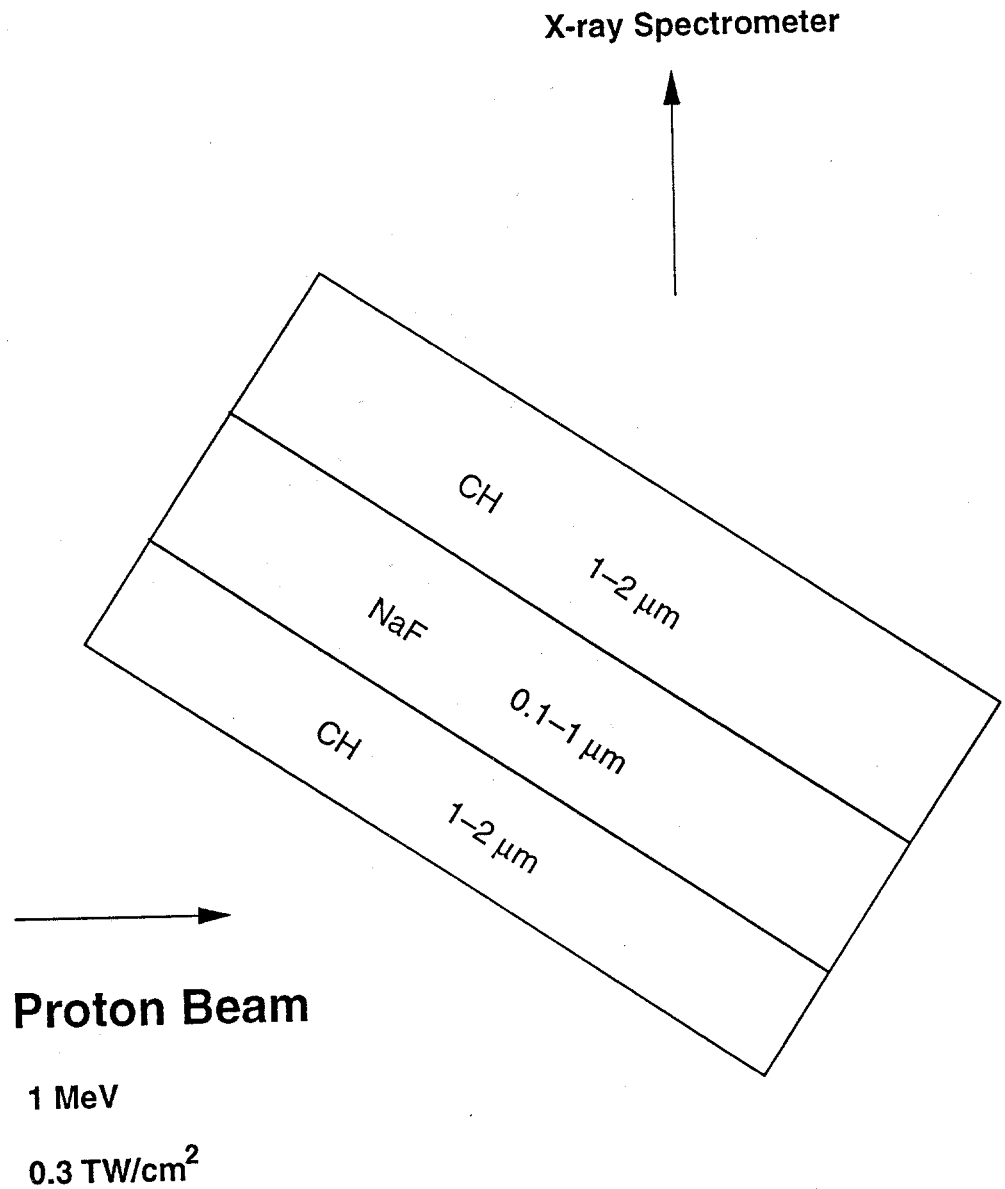

Figure 4. Schematic illustration of plastic sandwich target with a thin F tracer for diagnosing target temperatures and densities.

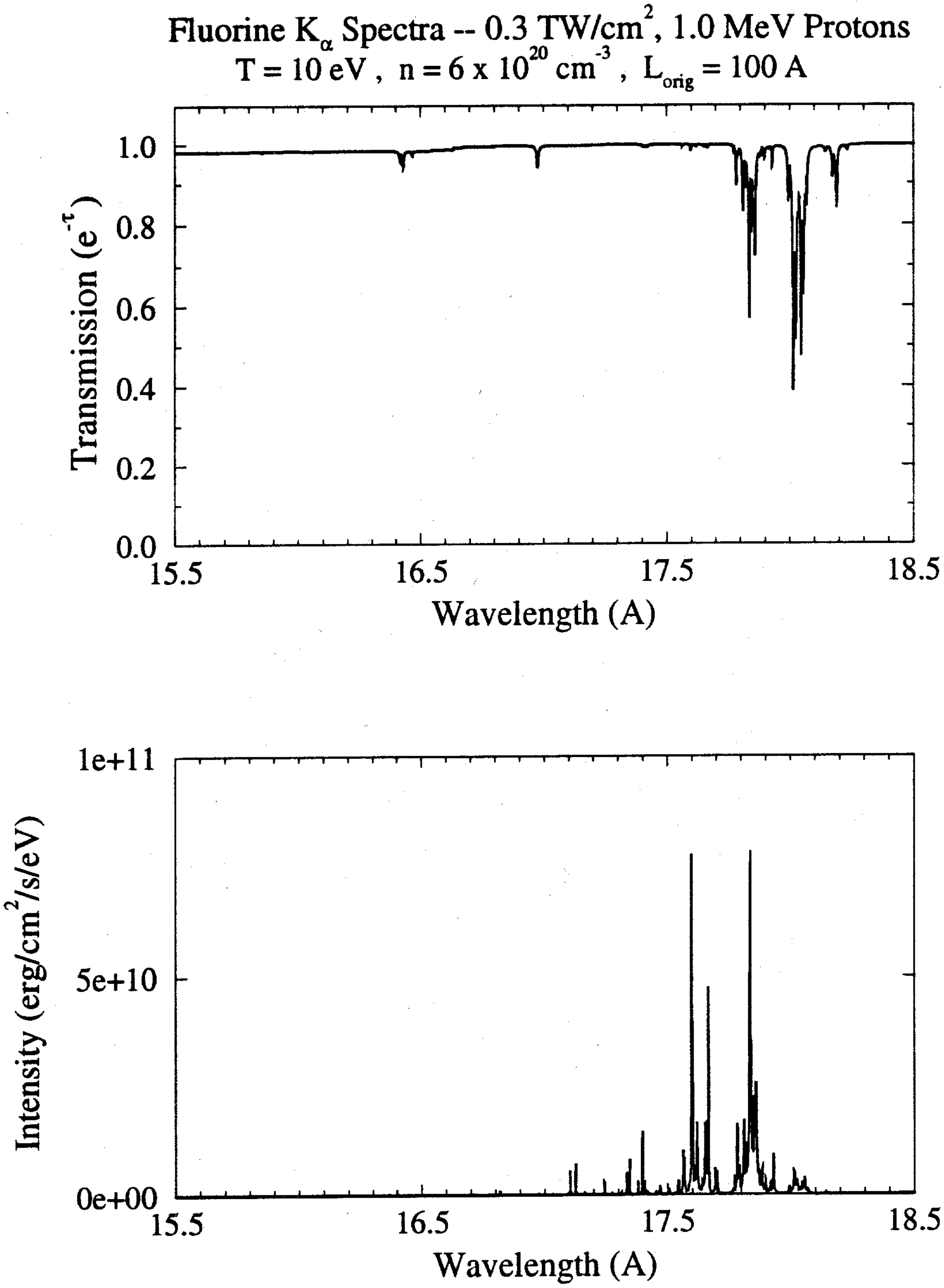

Figure 5(a). Fluorine K_α absorption (top) and emission (bottom) spectra for $T = 10$ eV, $n = 6 \times 10^{20}\,\mathrm{cm}^{-3}$, and $L_o = 100$ Å. The calculation assumes a 1.0 MeV, 0.3 TW/cm^2 proton beam.

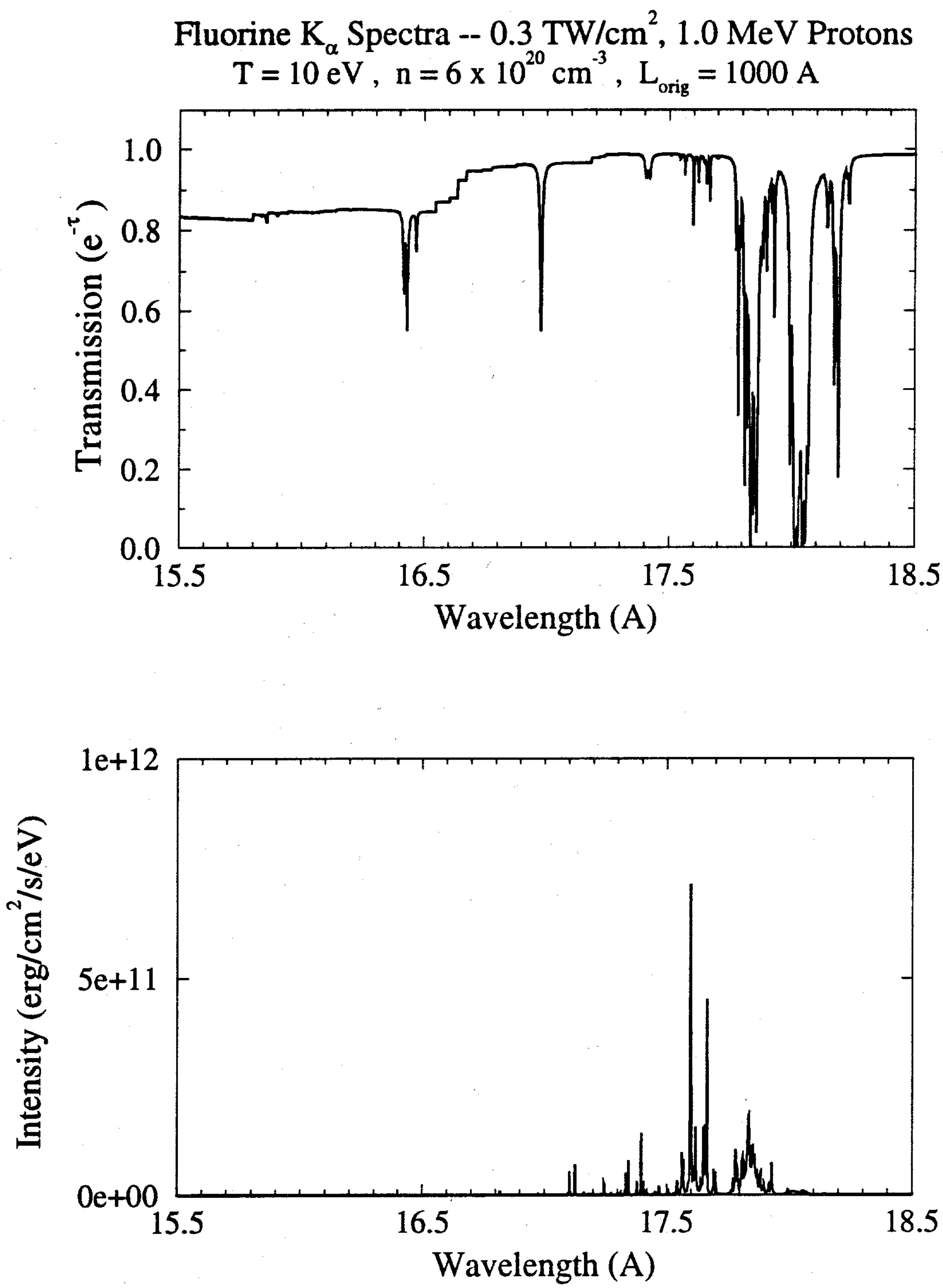

Figure 5(b). Fluorine K_α absorption (top) and emission (bottom) spectra for $T = 10$ eV, $n = 6 \times 10^{20}\,\mathrm{cm}^{-3}$, and $L_o = 1000$ Å. The calculation assumes a 1.0 MeV, 0.3 TW/cm^2 proton beam.

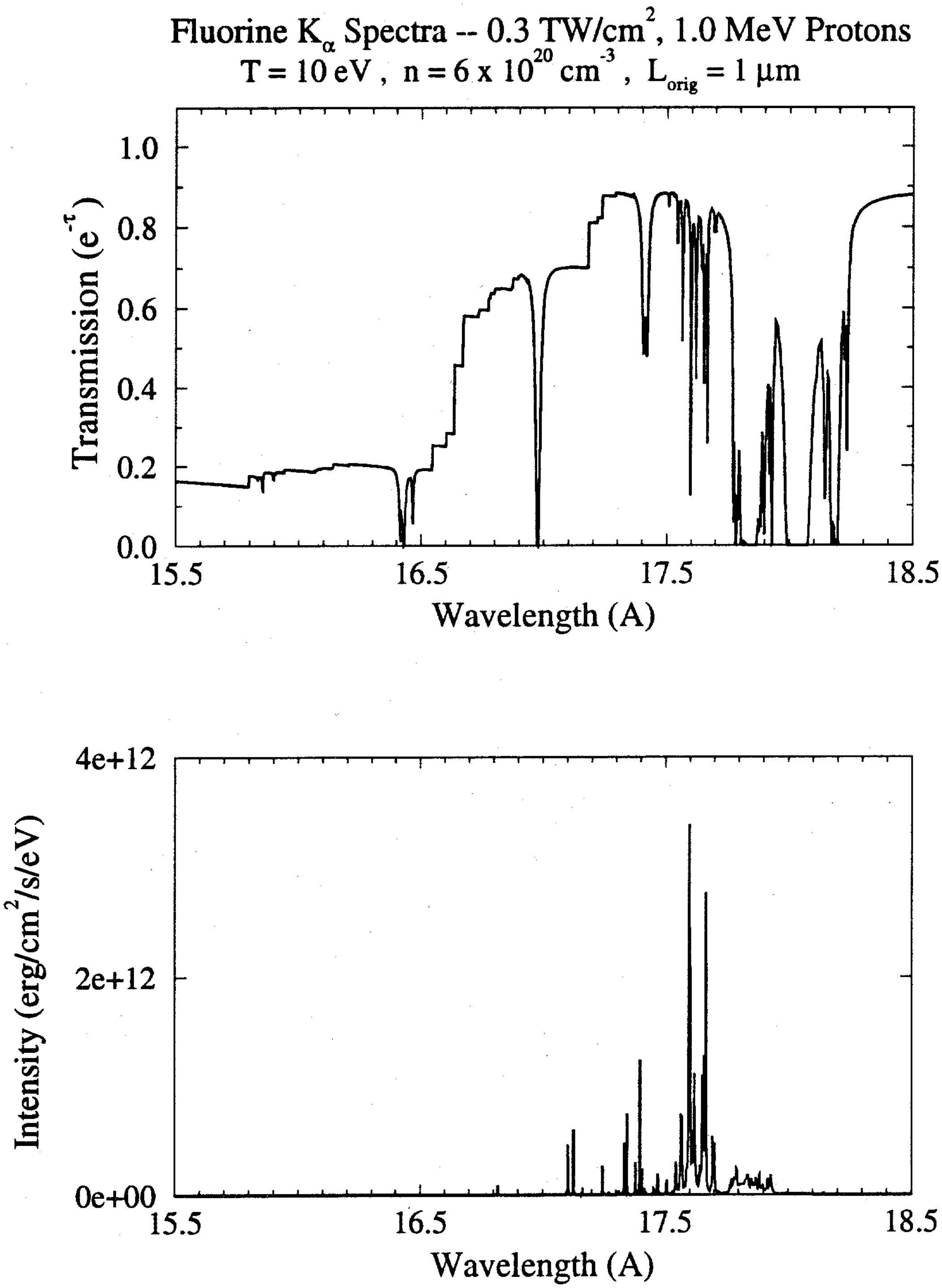

Figure 5(c). Fluorine K_α absorption (top) and emission (bottom) spectra for $T = 10$ eV, $n = 6 \times 10^{20}\,\mathrm{cm}^{-3}$, and $L_o = 1\,\mu$m. The calculation assumes a 1.0 MeV, 0.3 TW/cm^2 proton beam.

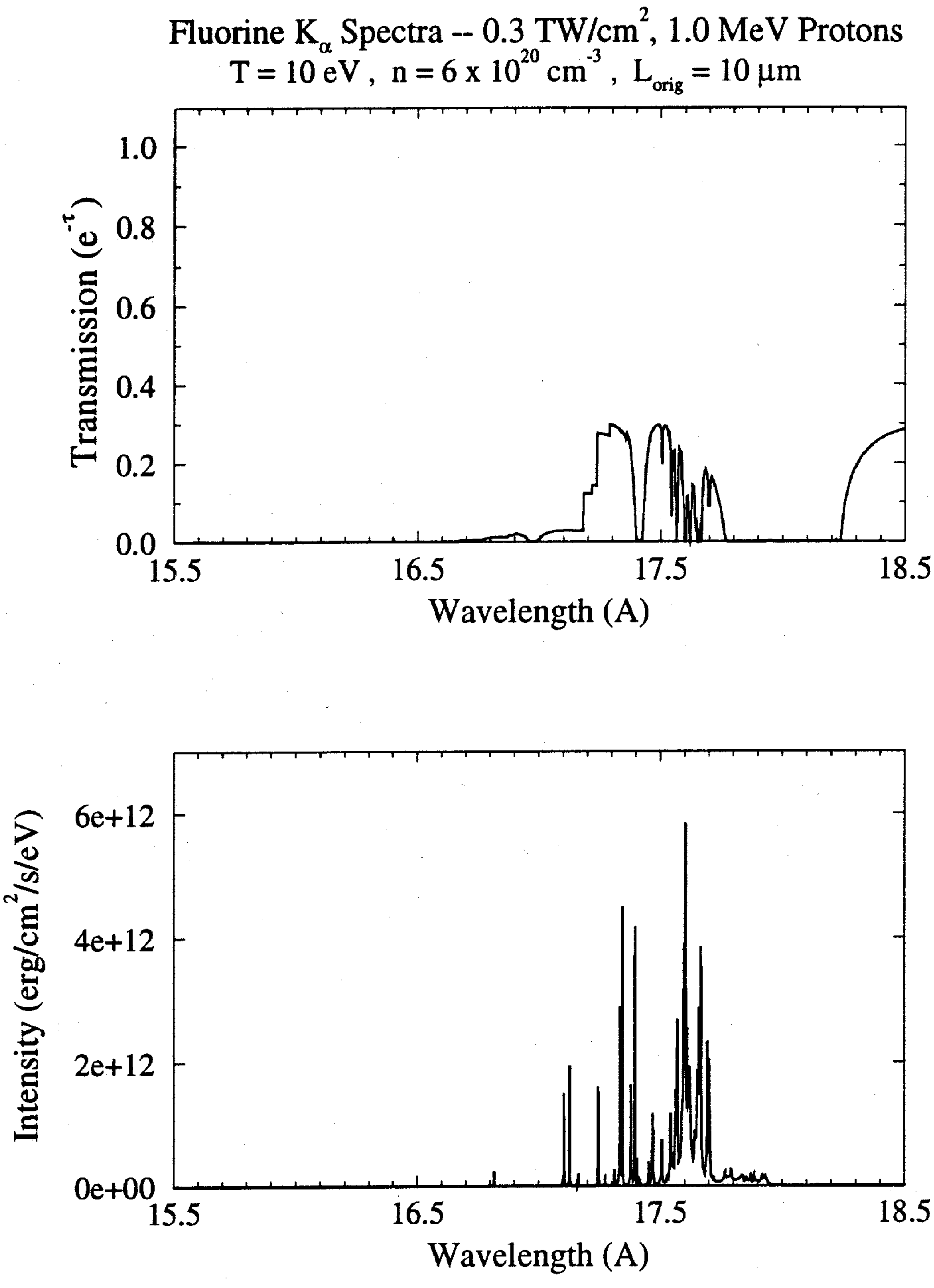

Figure 5(d). Fluorine K_α absorption (top) and emission (bottom) spectra for $T = 10$ eV, $n = 6 \times 10^{20}\,\mathrm{cm}^{-3}$, and $L_o = 10\,\mu$m. The calculation assumes a 1.0 MeV, 0.3 TW/cm^2 proton beam.

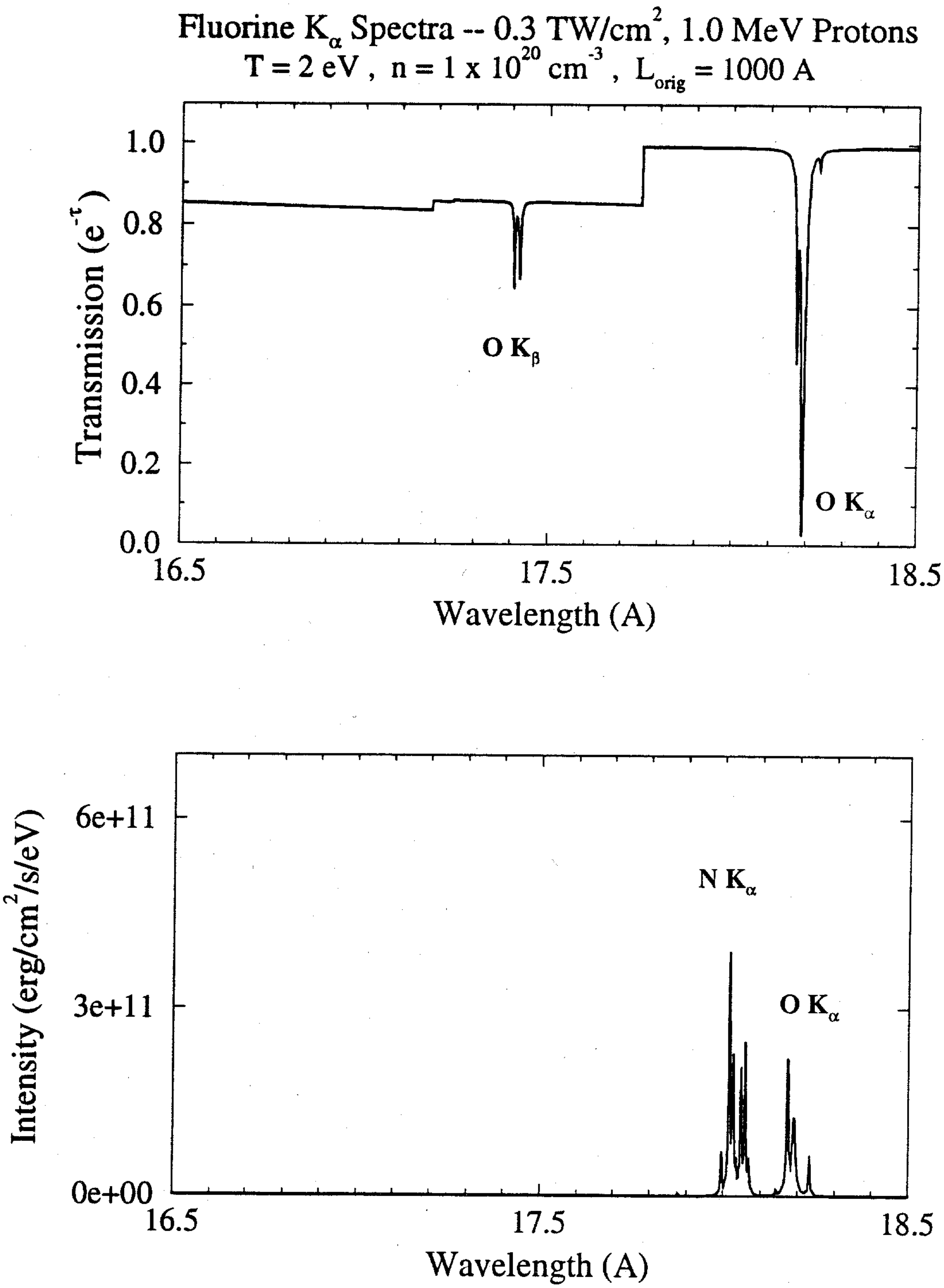

Figure 6(a). Fluorine K_α absorption (top) and emission (bottom) spectra for T = 2 eV, $n = 1 \times 10^{20}\,\mathrm{cm}^{-3}$, and L_o = 1000 Å. The calculation assumes a 1.0 MeV, 0.3 TW/cm^2 proton beam.

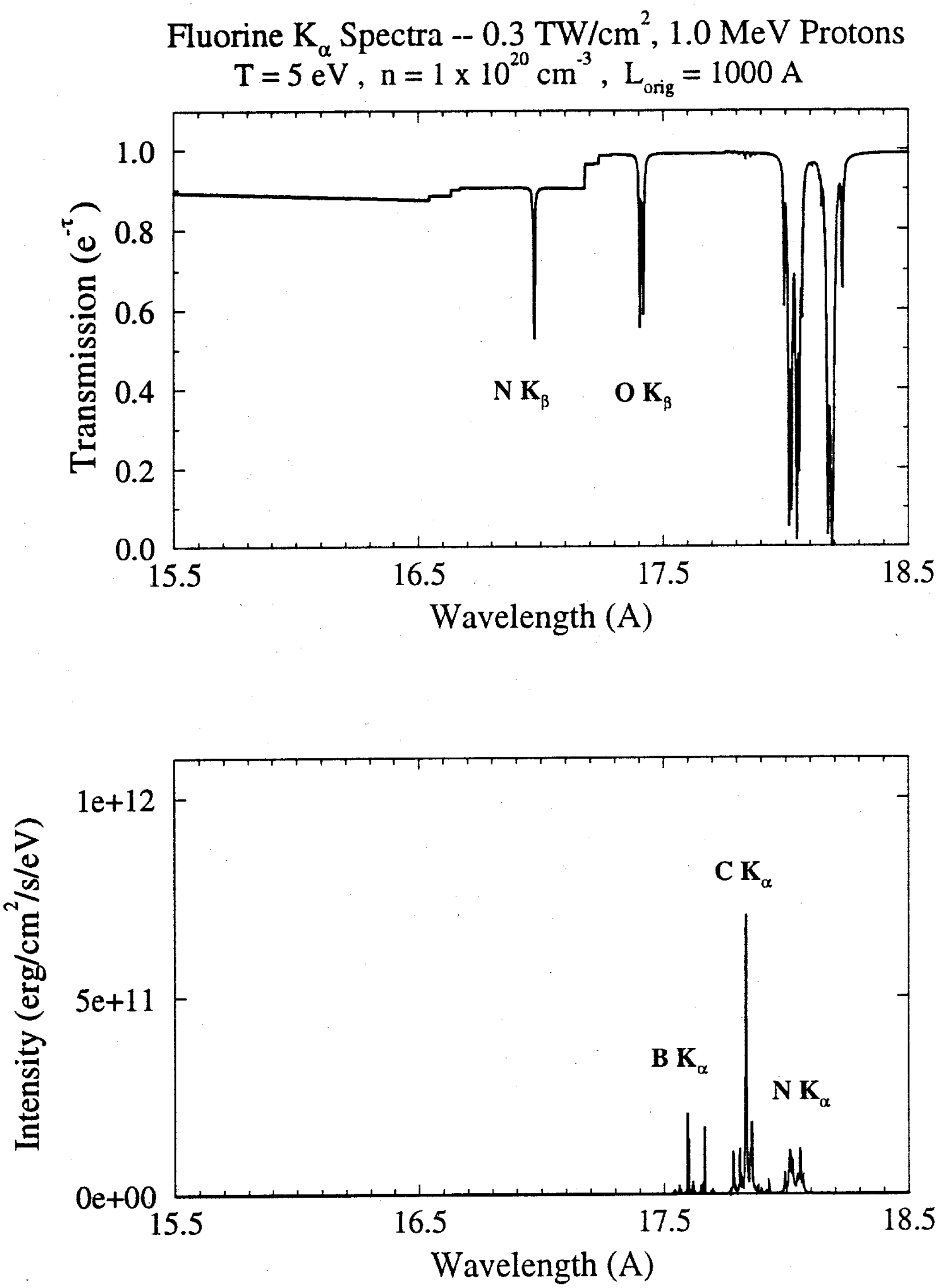

Figure 6(b). Fluorine K$_\alpha$ absorption (top) and emission (bottom) spectra for T = 5 eV, $n = 1 \times 10^{20}\,\mathrm{cm}^{-3}$, and L_o = 1000 Å. The calculation assumes a 1.0 MeV, 0.3 TW/cm^2 proton beam.

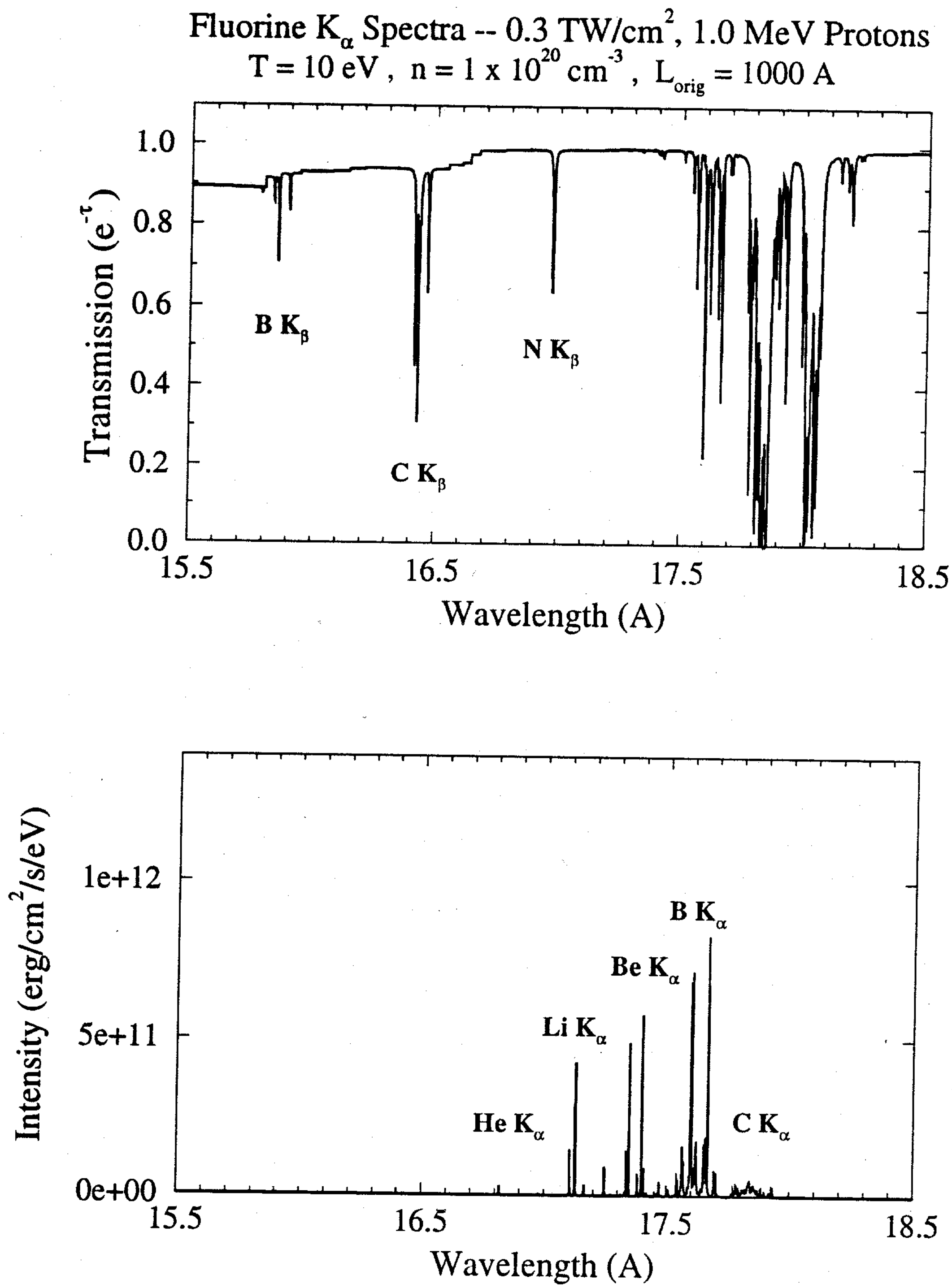

Figure 6(c). Fluorine K_α absorption (top) and emission (bottom) spectra for $T = 10$ eV, $n = 1 \times 10^{20}\,\mathrm{cm}^{-3}$, and $L_o = 1000$ Å. The calculation assumes a 1.0 MeV, 0.3 TW/cm^2 proton beam.

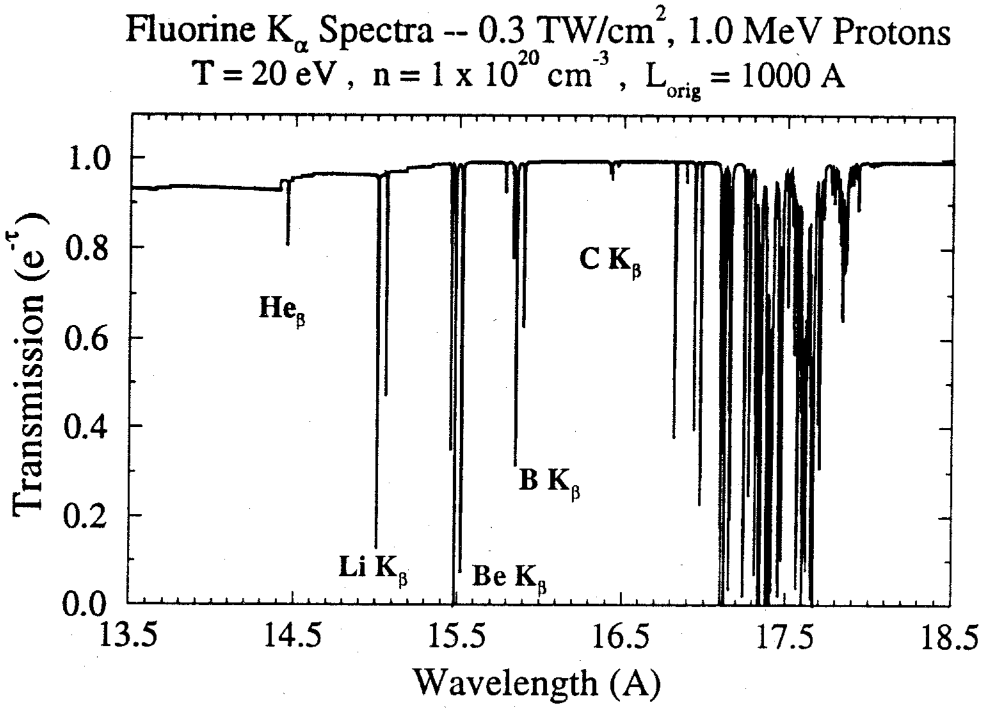

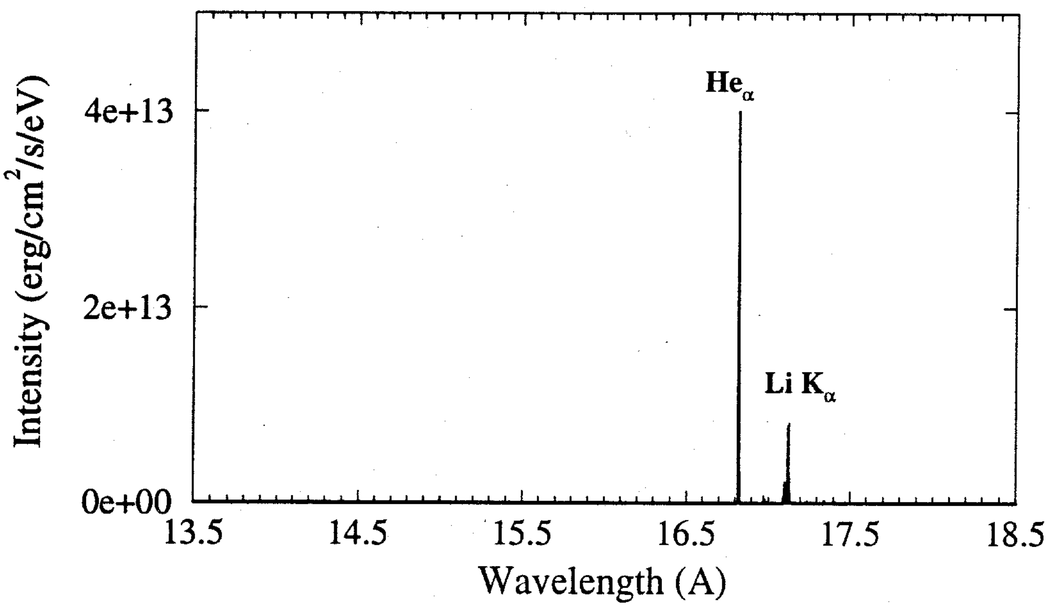

Figure 6(d). Fluorine K_α absorption (top) and emission (bottom) spectra for $T = 20$ eV, $n = 1 \times 10^{20}\,\text{cm}^{-3}$, and $L_o = 1000$ Å. The calculation assumes a 1.0 MeV, 0.3 TW/cm^2 proton beam.

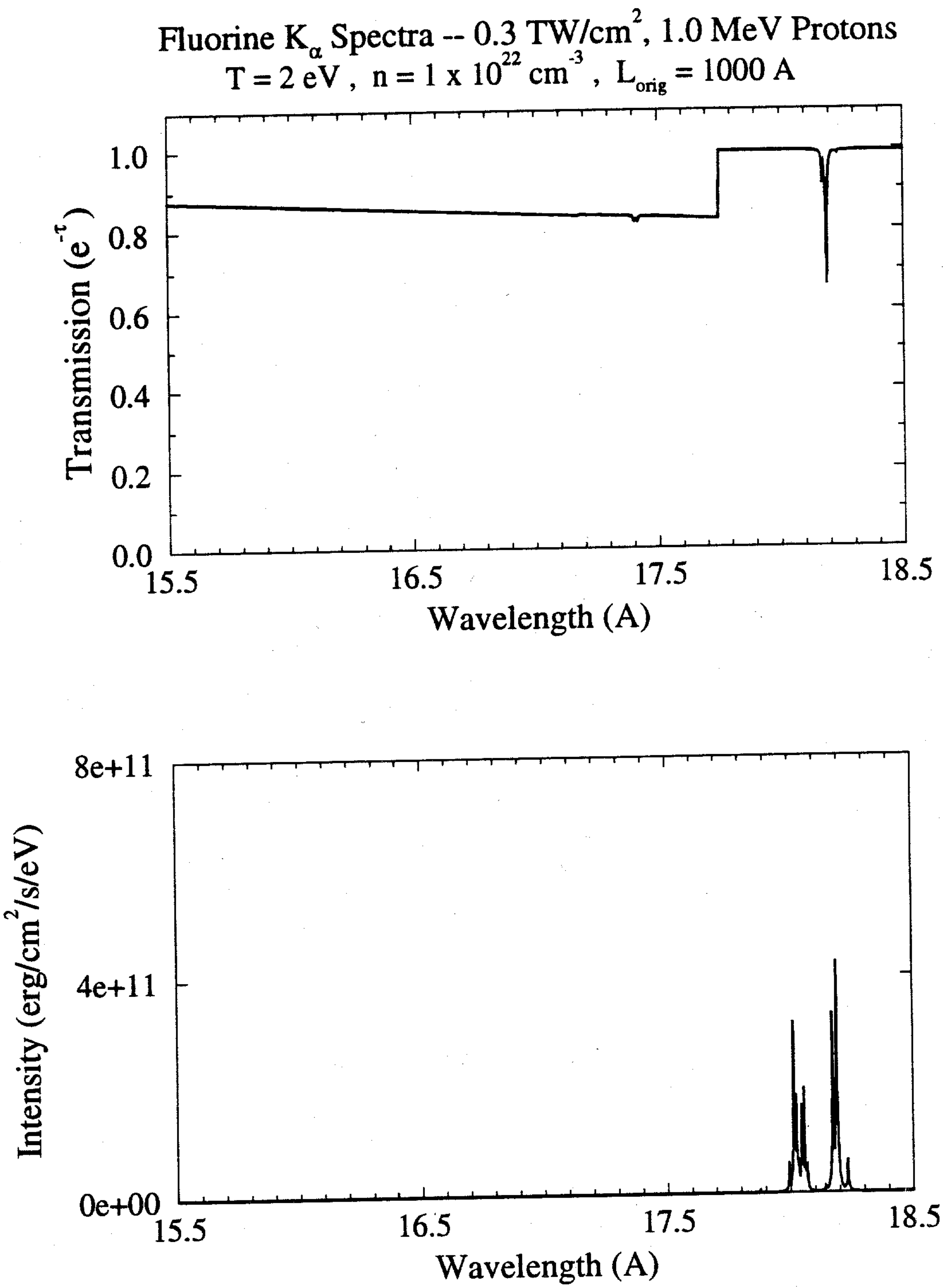

Figure 7(a). Fluorine K$_\alpha$ absorption (top) and emission (bottom) spectra for $T = 2$ eV, $n = 1 \times 10^{22}\,\mathrm{cm}^{-3}$, and $L_o = 1000$ Å. The calculation assumes a 1.0 MeV, 0.3 TW/cm^2 proton beam.

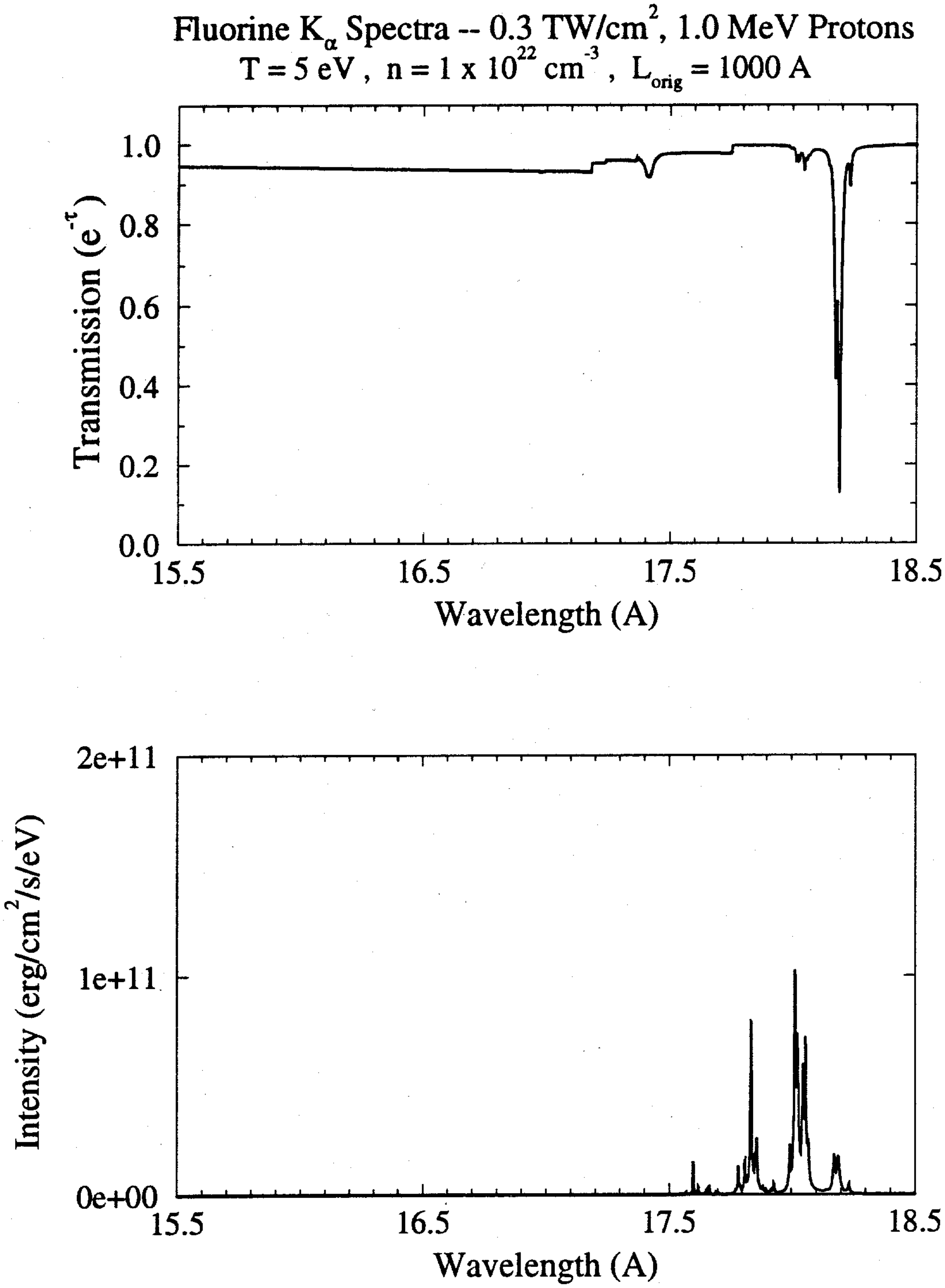

Figure 7(b). Fluorine K_α absorption (top) and emission (bottom) spectra for $T = 5$ eV, $n = 1 \times 10^{22}\,\mathrm{cm}^{-3}$, and $L_o = 1000$ Å. The calculation assumes a 1.0 MeV, 0.3 TW/cm^2 proton beam.

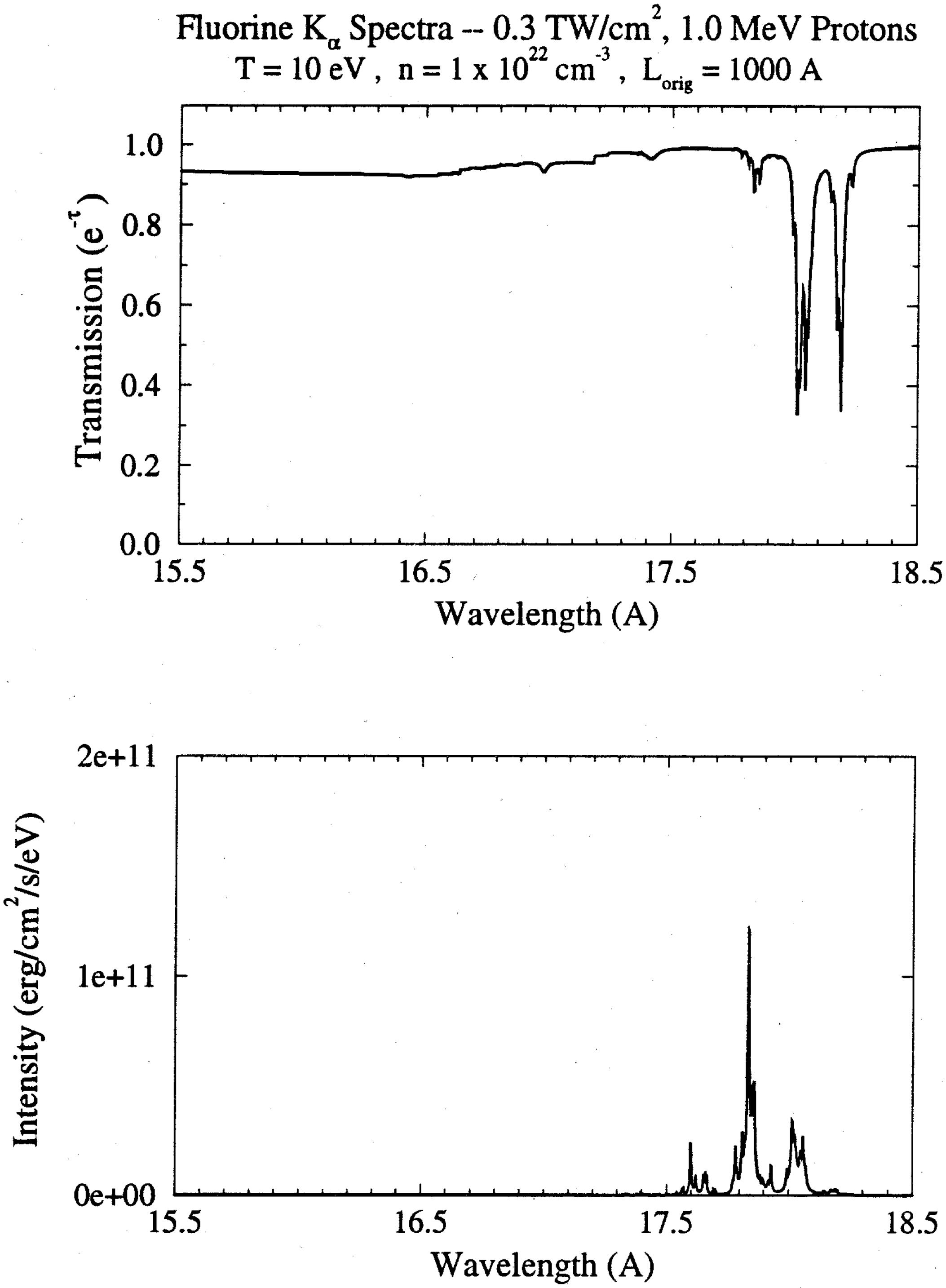

Figure 7(c). Fluorine K_α absorption (top) and emission (bottom) spectra for $T = 10$ eV, $n = 1 \times 10^{22}\,\mathrm{cm}^{-3}$, and $L_o = 1000$ Å. The calculation assumes a 1.0 MeV, 0.3 TW/cm^2 proton beam.

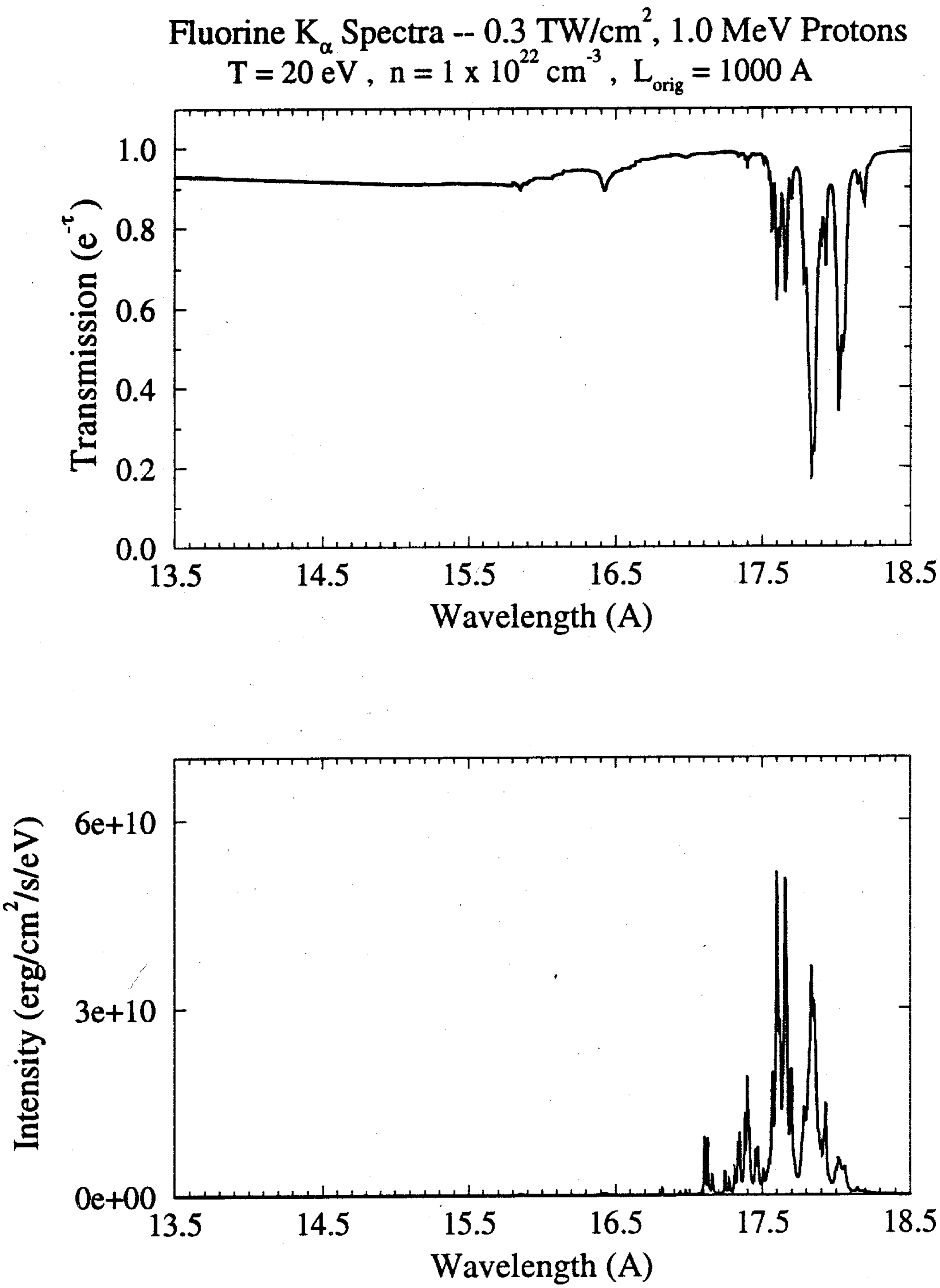

Figure 7(d). Fluorine K_α absorption (top) and emission (bottom) spectra for T = 20 eV, $n = 1 \times 10^{22}\,\mathrm{cm}^{-3}$, and L_o = 1000 Å. The calculation assumes a 1.0 MeV, 0.3 TW/cm^2 proton beam.

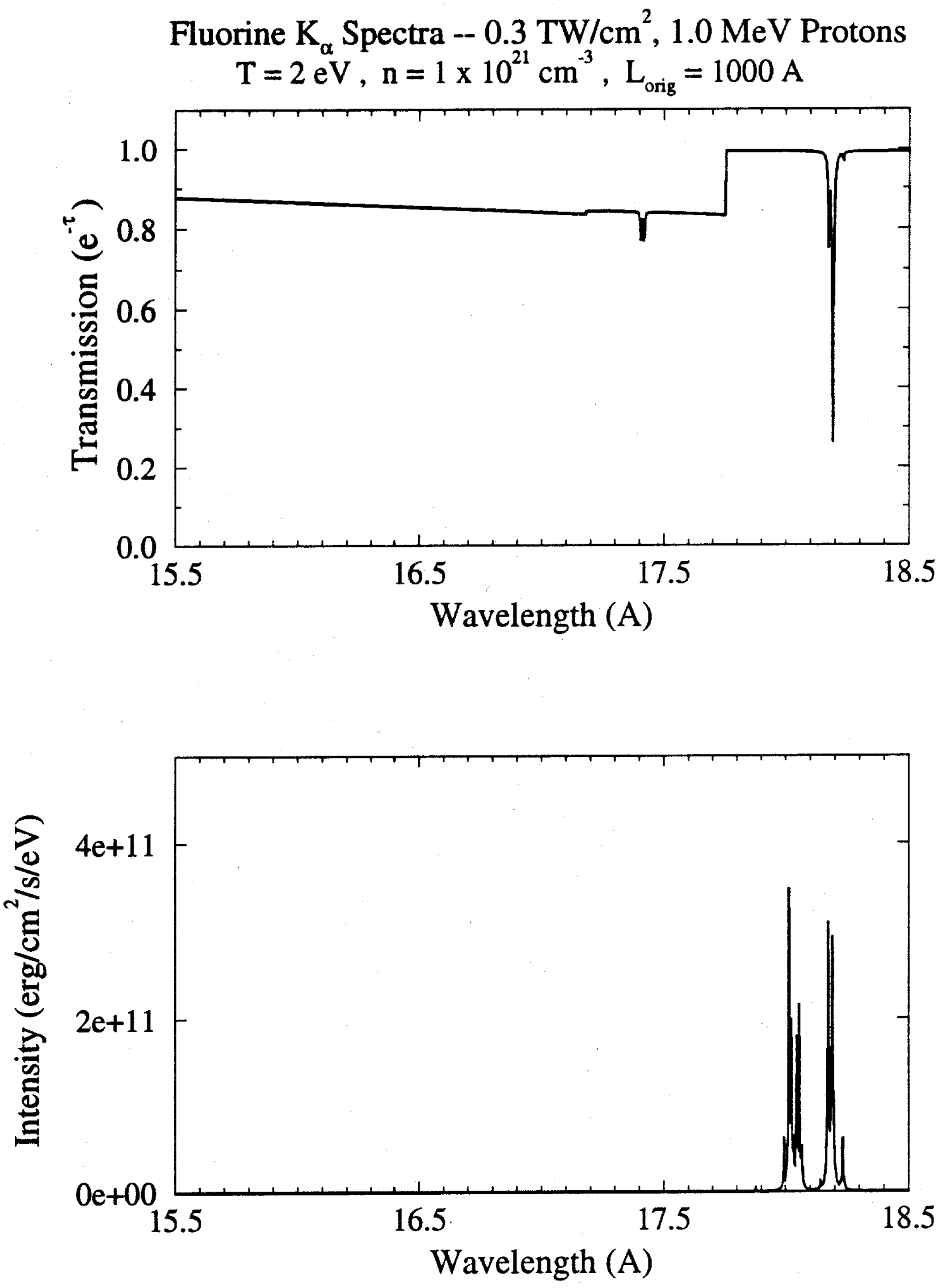

Figure 8(a). Fluorine K_α absorption (top) and emission (bottom) spectra for $T = 2$ eV, $n = 1 \times 10^{21}\,\mathrm{cm}^{-3}$, and $L_o = 1000$ Å. The calculation assumes a 1.0 MeV, 0.3 TW/cm^2 proton beam.

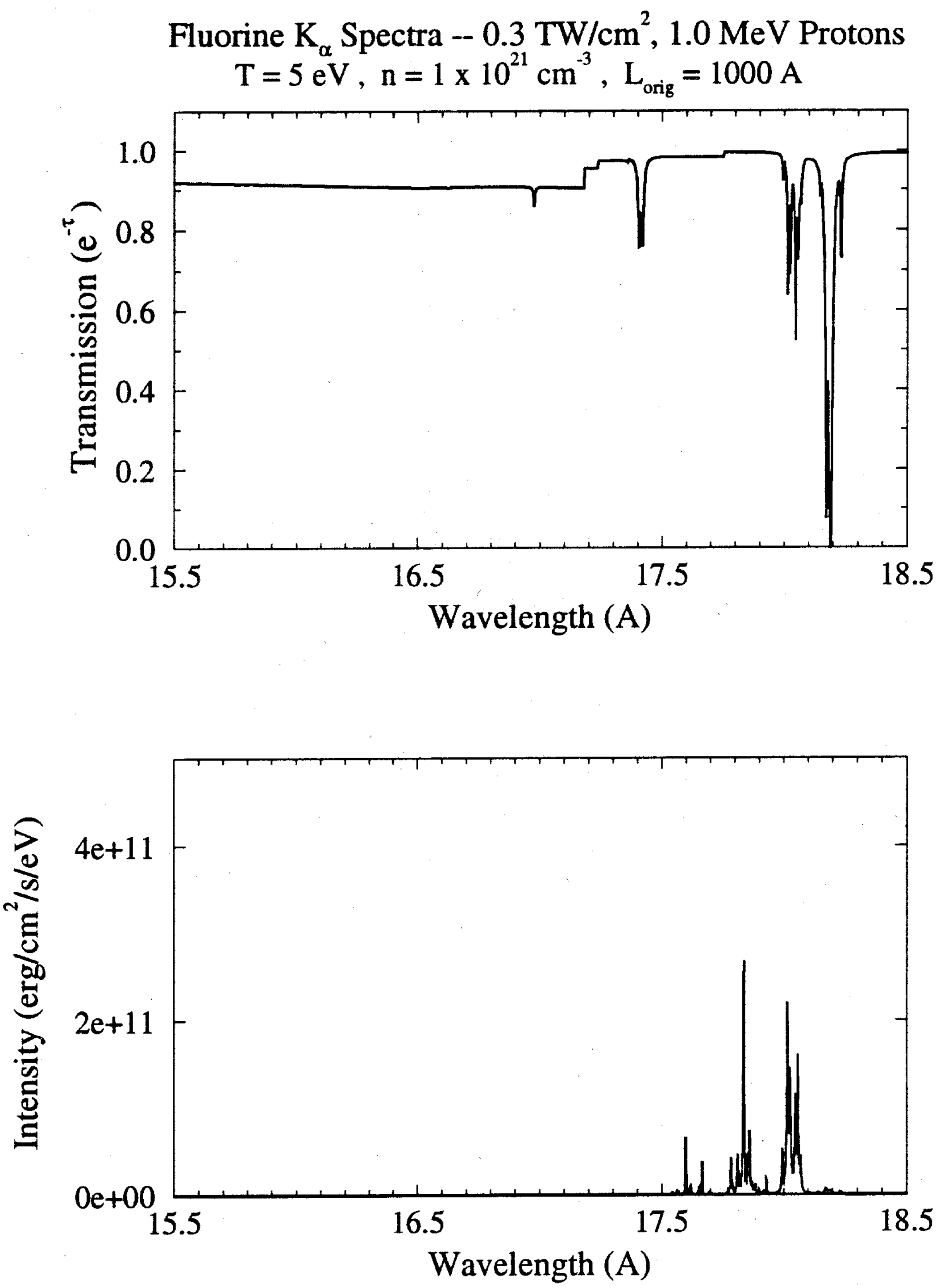

Figure 8(b). Fluorine K_α absorption (top) and emission (bottom) spectra for $T = 5$ eV, $n = 1 \times 10^{21}\,\mathrm{cm}^{-3}$, and $L_o = 1000$ Å. The calculation assumes a 1.0 MeV, 0.3 TW/cm^2 proton beam.

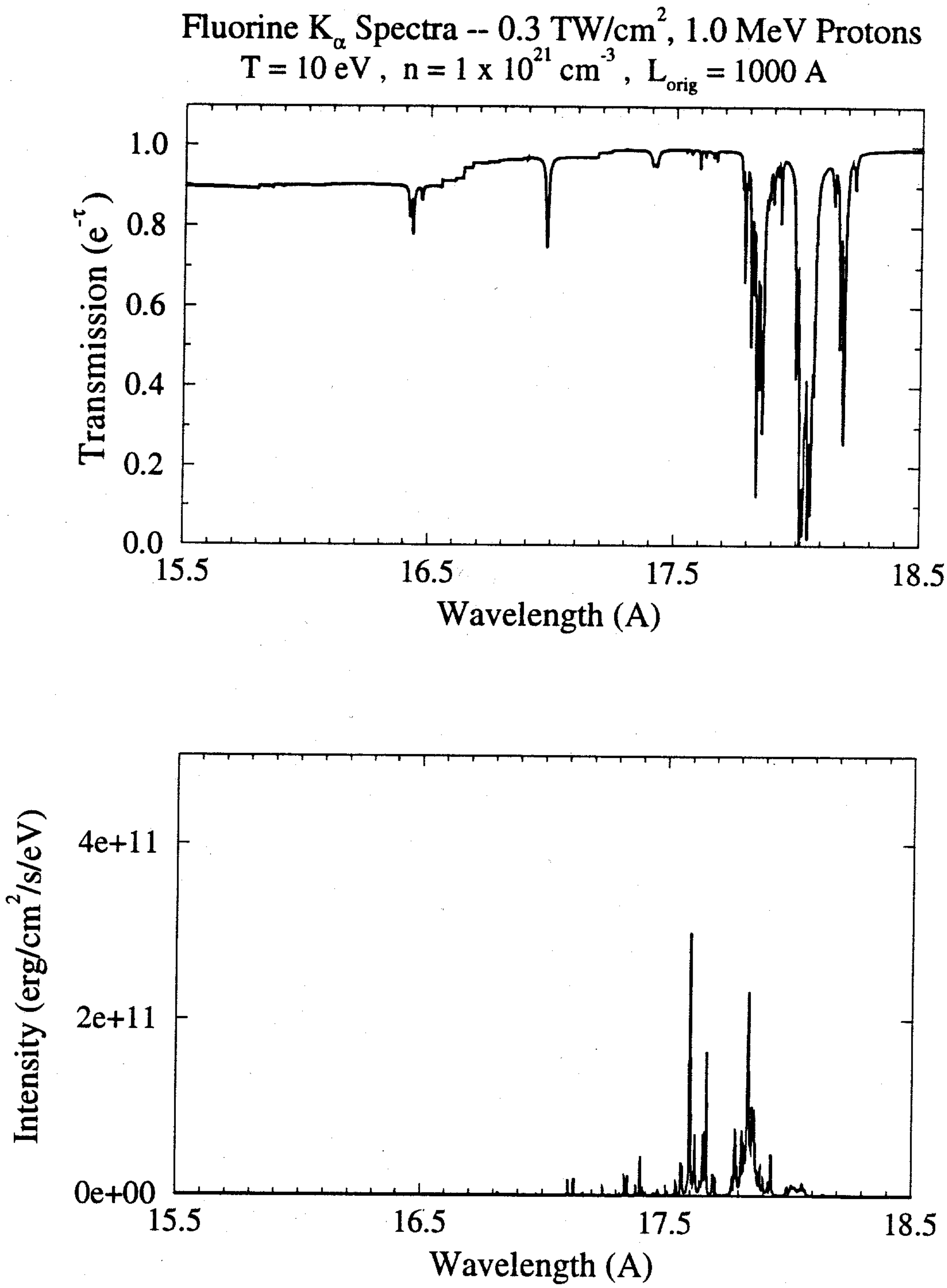

Figure 8(c). Fluorine K_α absorption (top) and emission (bottom) spectra for $T = 10$ eV, $n = 1 \times 10^{21}\,\mathrm{cm}^{-3}$, and $L_o = 1000$ Å. The calculation assumes a 1.0 MeV, 0.3 TW/cm^2 proton beam.

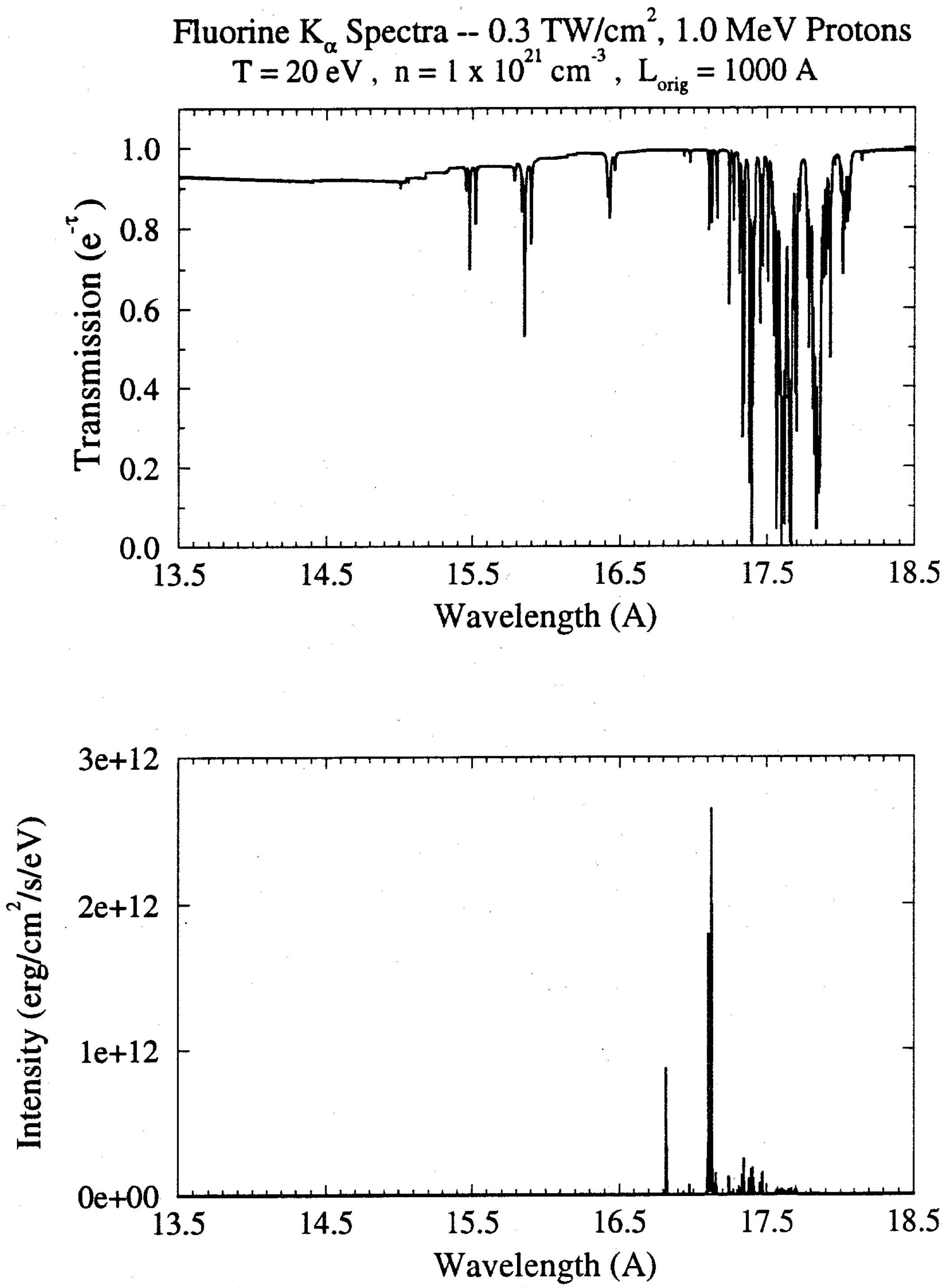

Figure 8(d). Fluorine K_α absorption (top) and emission (bottom) spectra for T = 20 eV, $n = 1 \times 10^{21}\,\mathrm{cm}^{-3}$, and L_o = 1000 Å. The calculation assumes a 1.0 MeV, 0.3 TW/cm^2 proton beam.

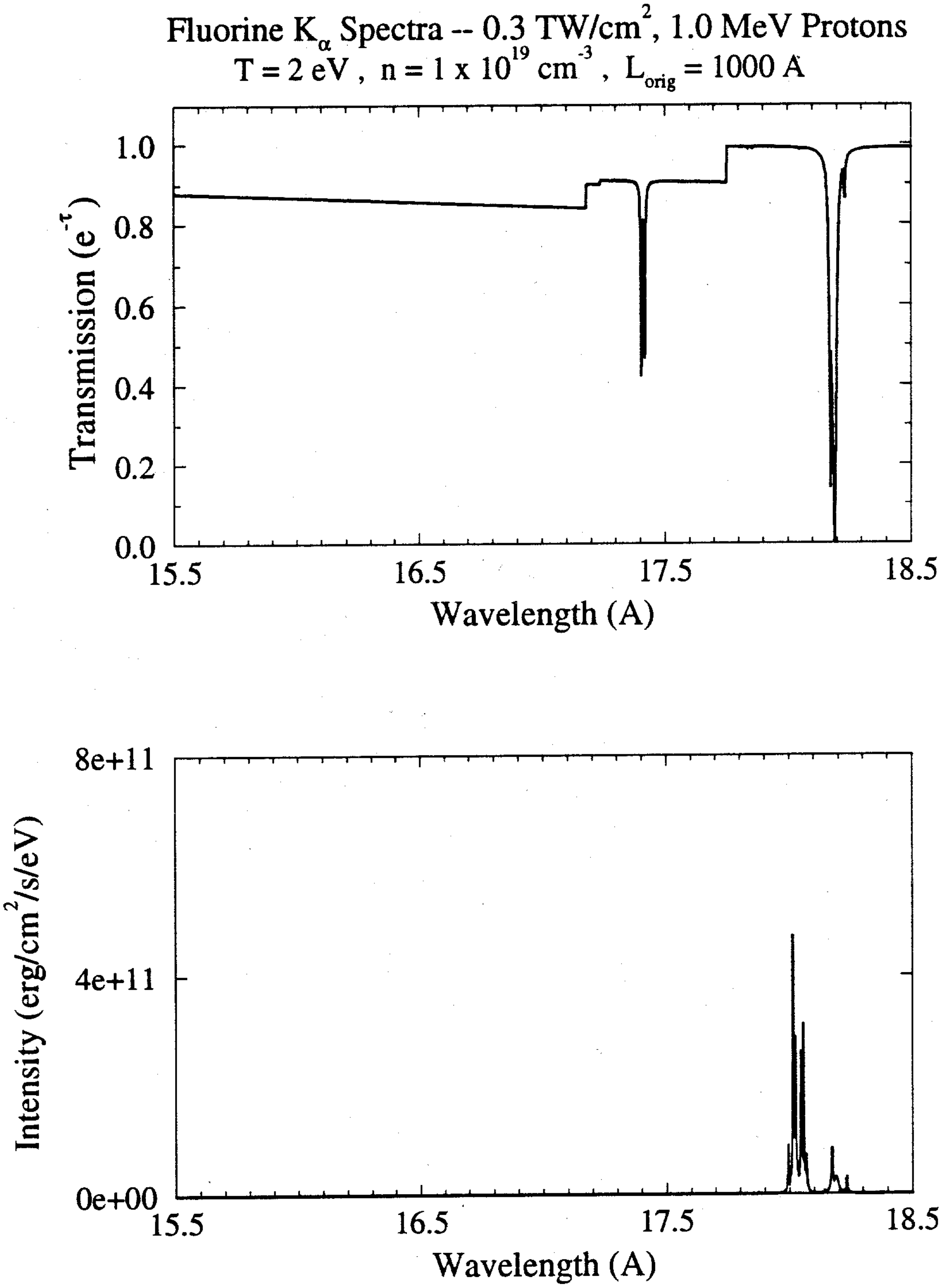

Figure 9(a). Fluorine K_α absorption (top) and emission (bottom) spectra for $T = 2$ eV, $n = 1 \times 10^{19}\,\mathrm{cm}^{-3}$, and $L_o = 1000$ Å. The calculation assumes a 1.0 MeV, 0.3 TW/cm^2 proton beam.

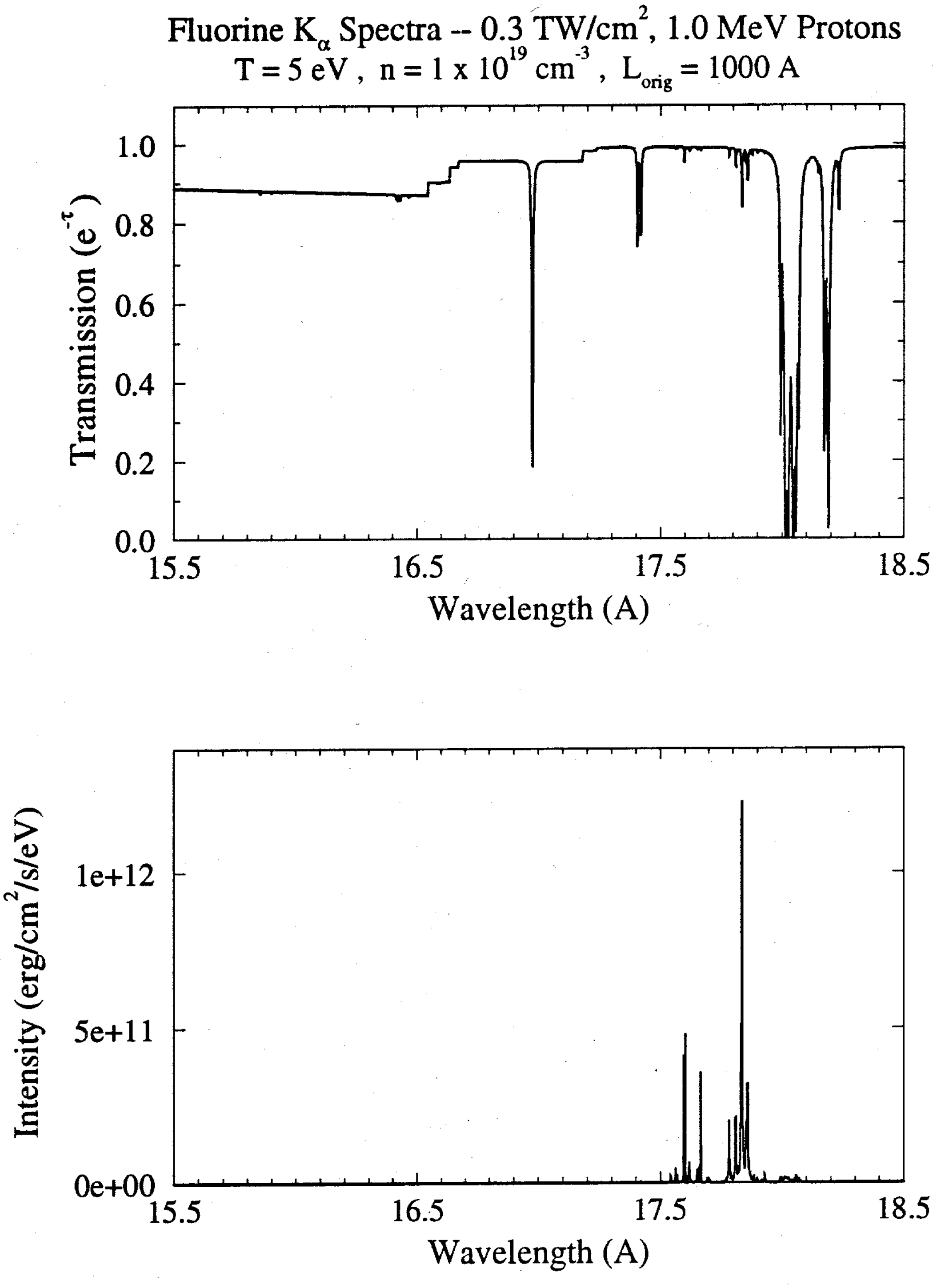

Figure 9(b). Fluorine K_α absorption (top) and emission (bottom) spectra for $T = 5$ eV, $n = 1 \times 10^{19}\,\mathrm{cm}^{-3}$, and $L_o = 1000$ Å. The calculation assumes a 1.0 MeV, 0.3 TW/cm^2 proton beam.

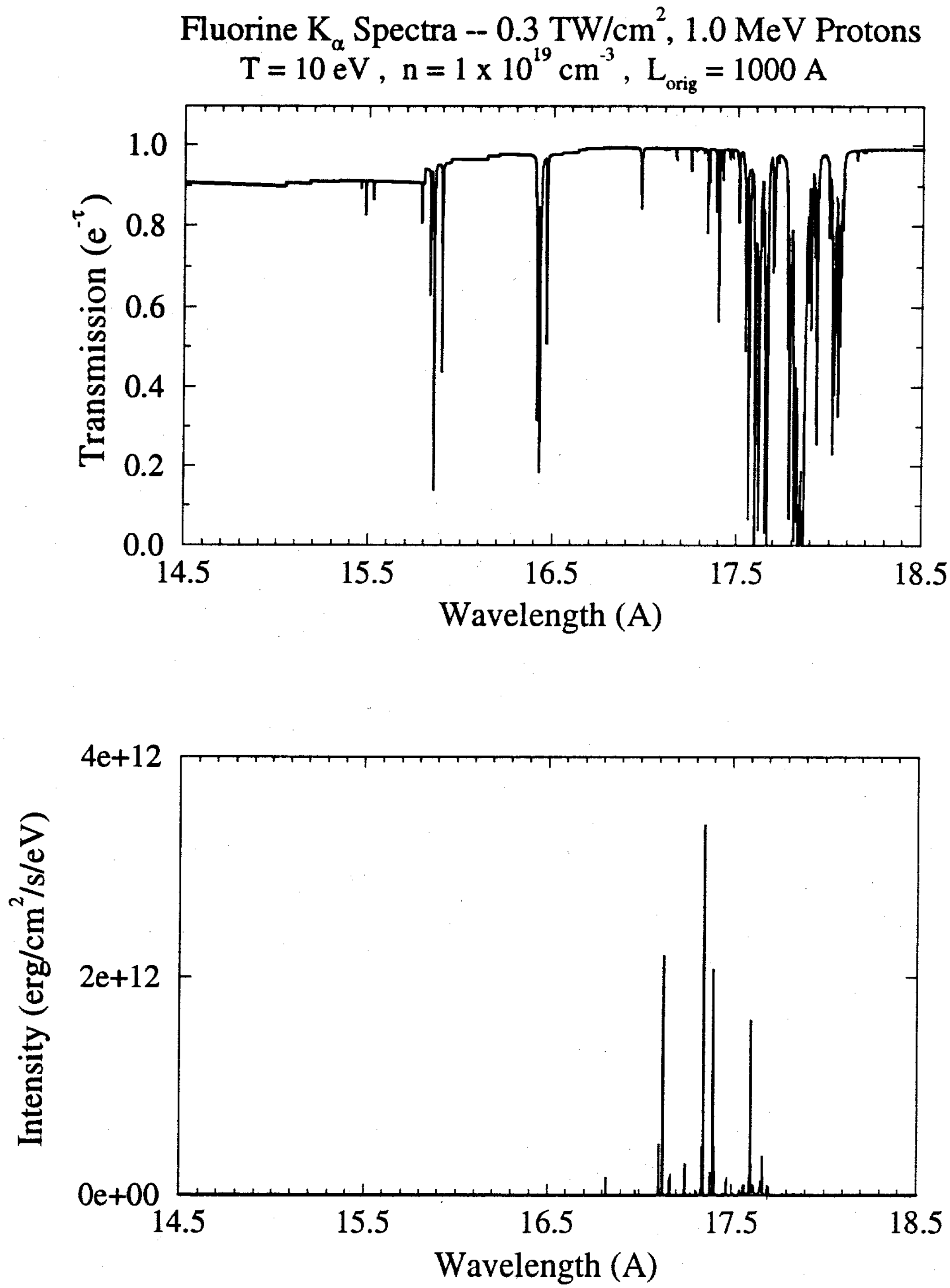

Figure 9(c). Fluorine K_α absorption (top) and emission (bottom) spectra for $T = 10$ eV, $n = 1 \times 10^{19}\,\mathrm{cm}^{-3}$, and $L_o = 1000$ Å. The calculation assumes a 1.0 MeV, 0.3 TW/cm^2 proton beam.

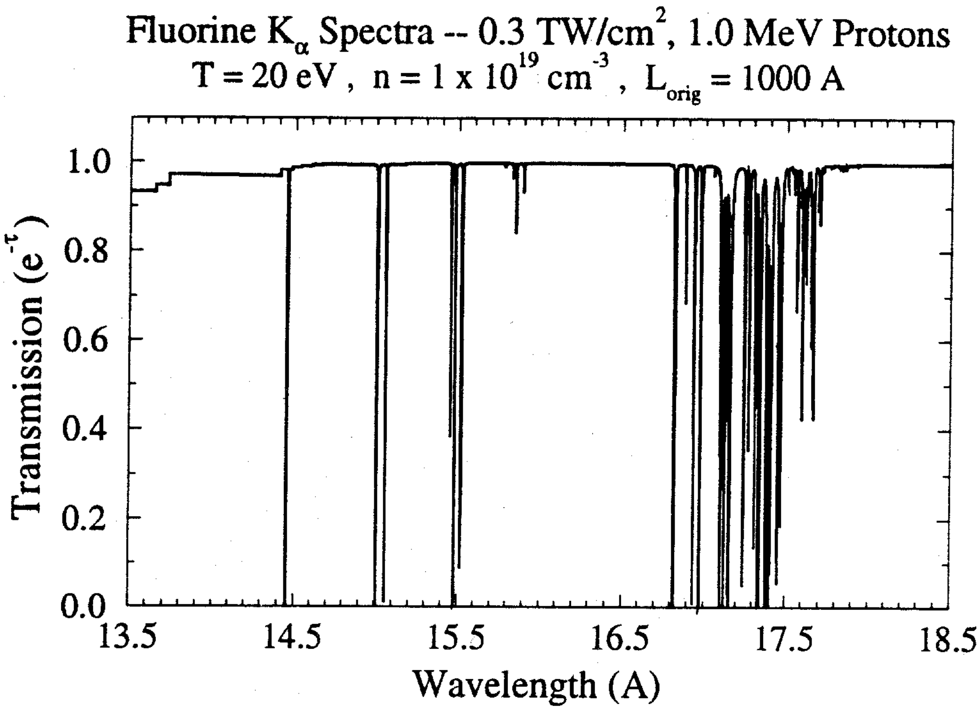

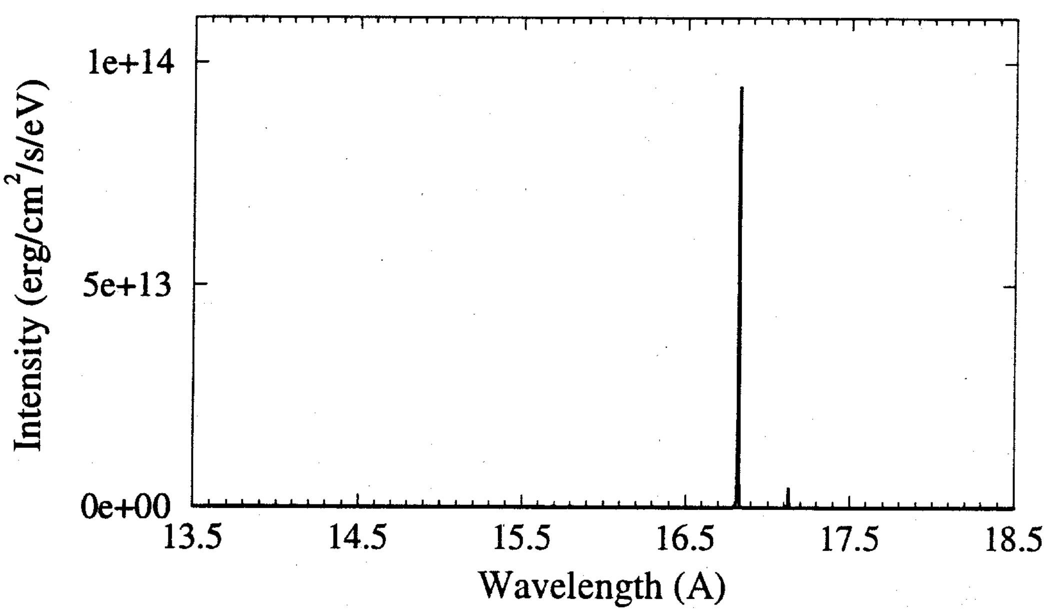

Figure 9(d). Fluorine K_α absorption (top) and emission (bottom) spectra for $T = 20$ eV, $n = 1 \times 10^{19}\,\mathrm{cm}^{-3}$, and $L_o = 1000$ Å. The calculation assumes a 1.0 MeV, 0.3 TW/cm^2 proton beam.

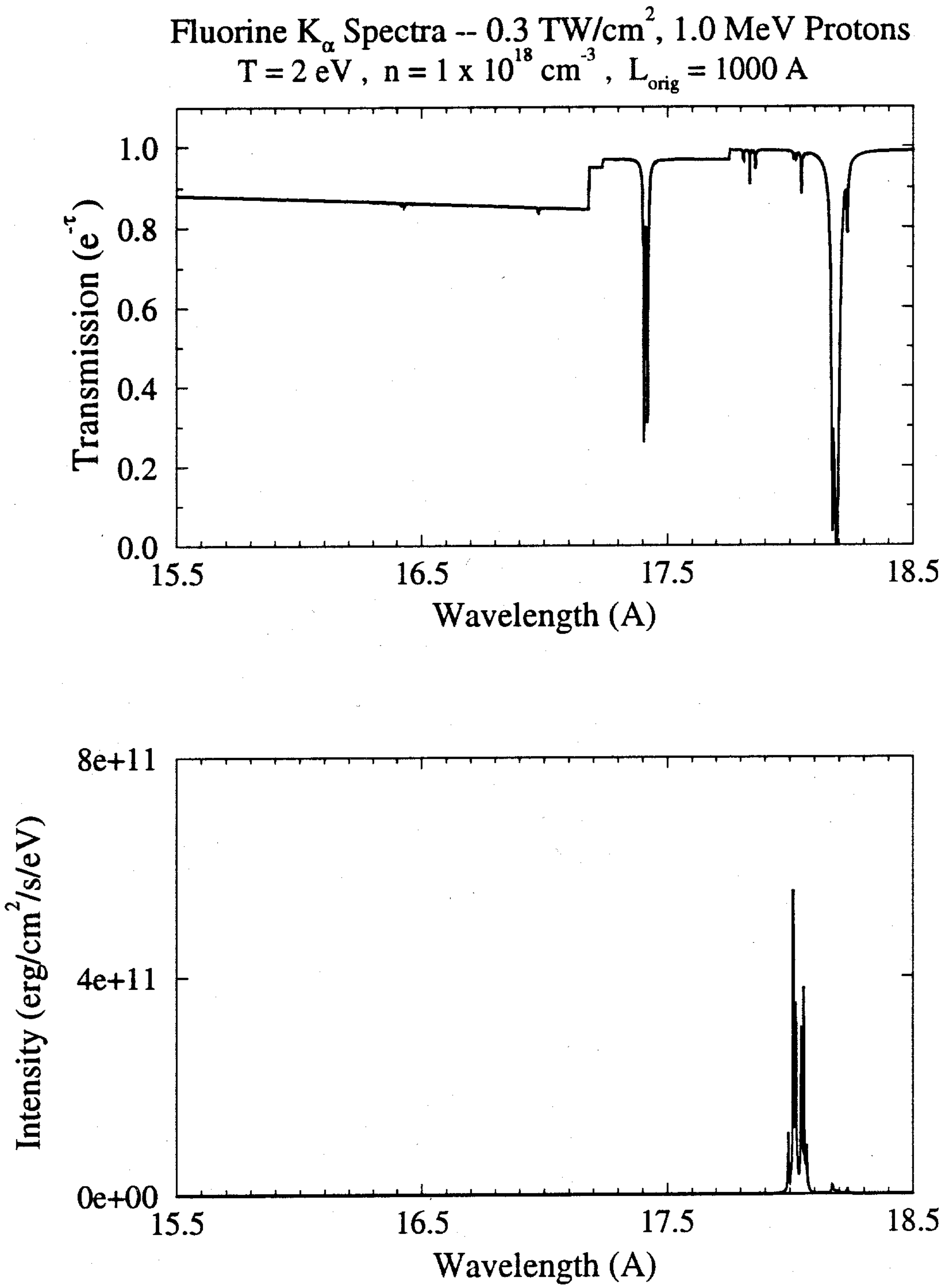

Figure 10(a). Fluorine K_α absorption (top) and emission (bottom) spectra for T = 2 eV, $n = 1 \times 10^{18}\,\mathrm{cm}^{-3}$, and L_o = 1000 Å. The calculation assumes a 1.0 MeV, 0.3 TW/cm^2 proton beam.

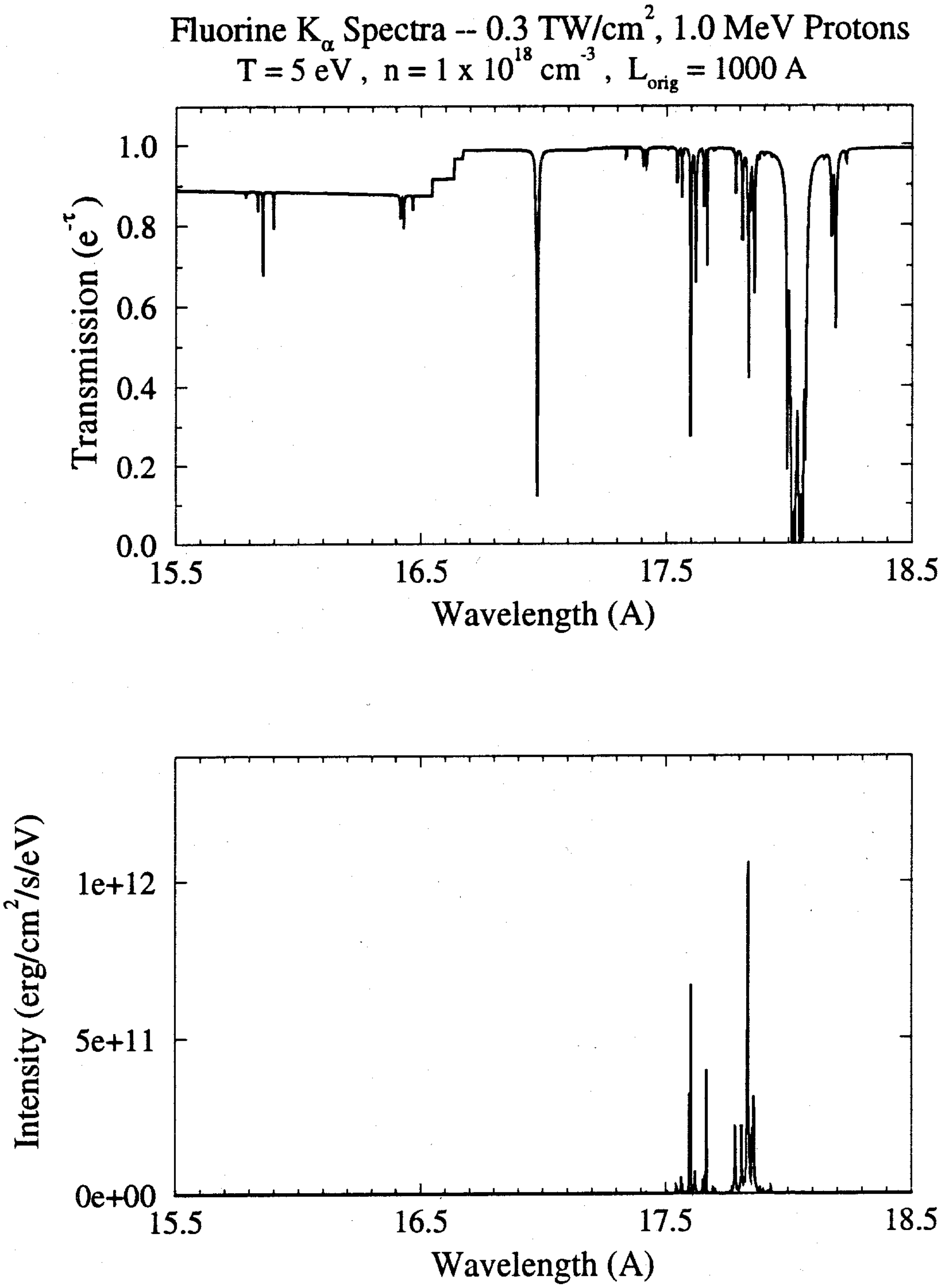

Figure 10(b). Fluorine K_α absorption (top) and emission (bottom) spectra for $T = 5$ eV, $n = 1 \times 10^{18}\,\mathrm{cm}^{-3}$, and $L_o = 1000$ Å. The calculation assumes a 1.0 MeV, 0.3 TW/cm^2 proton beam.

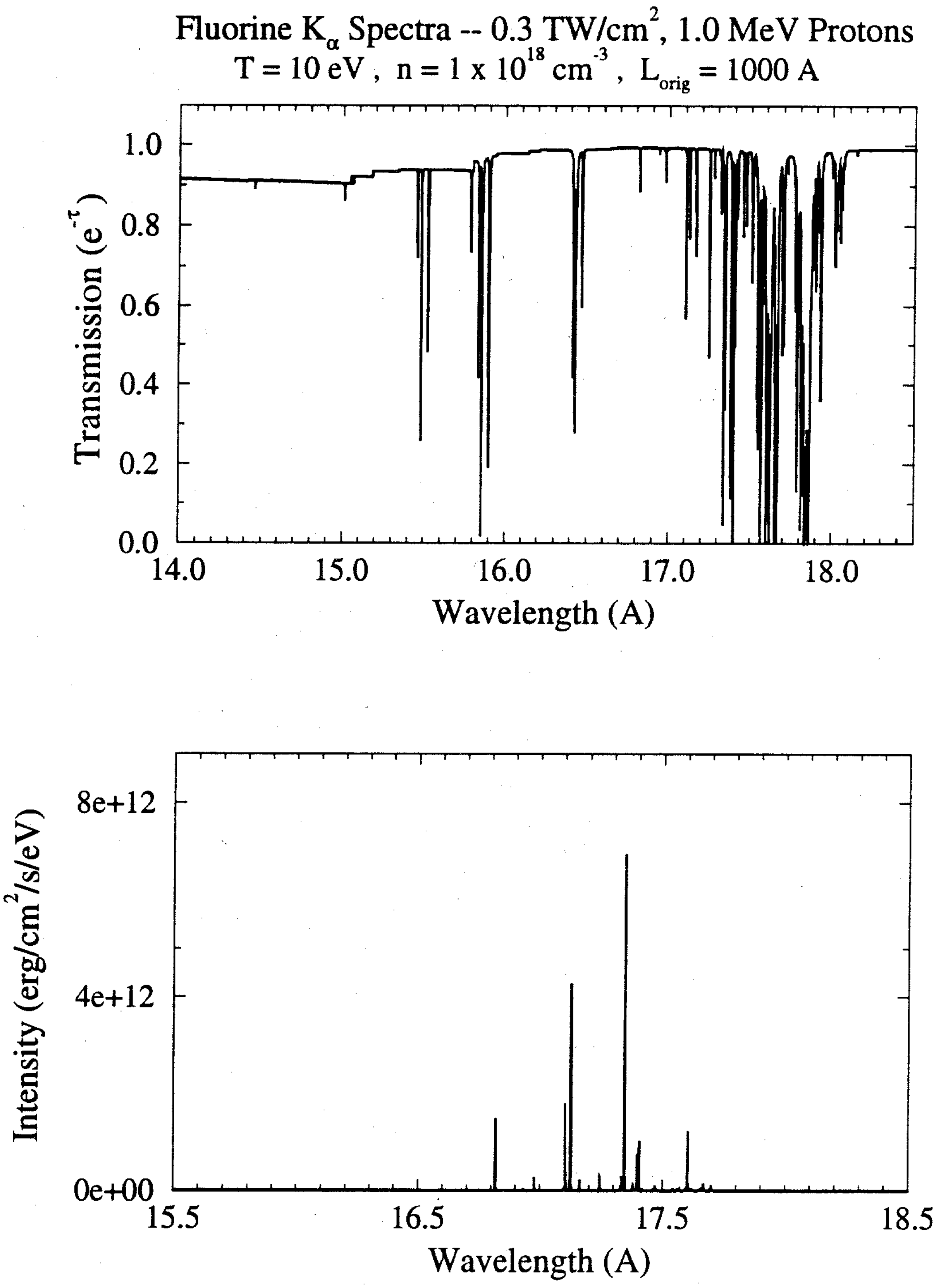

Figure 10(c). Fluorine K_α absorption (top) and emission (bottom) spectra for $T = 10$ eV, $n = 1 \times 10^{18}\,\mathrm{cm}^{-3}$, and $L_o = 1000$ Å. The calculation assumes a 1.0 MeV, 0.3 TW/cm^2 proton beam.

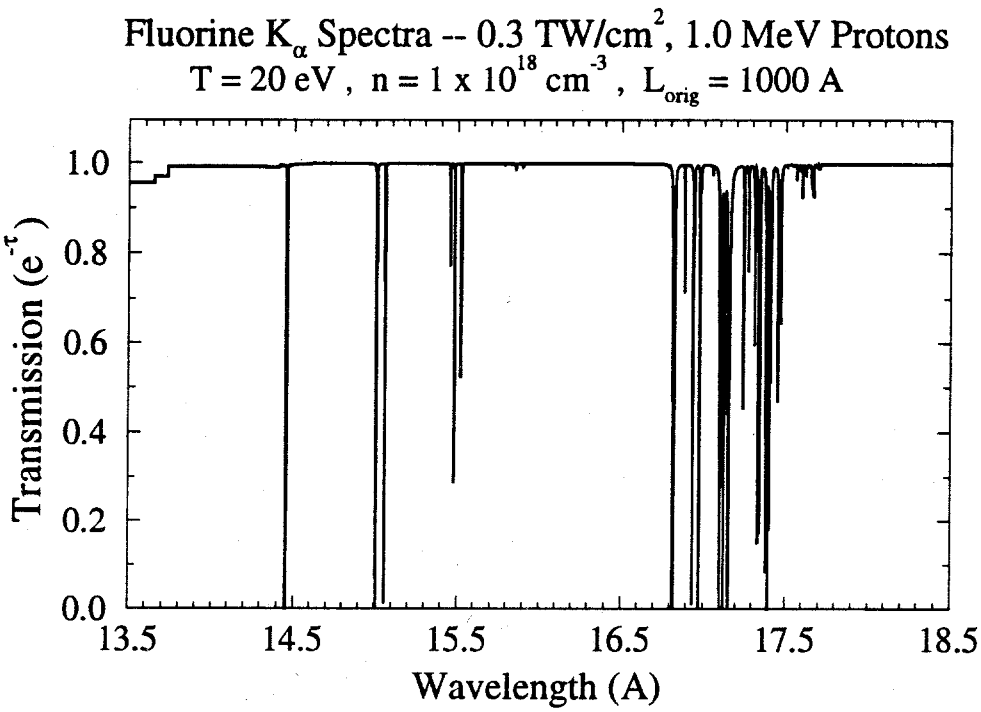

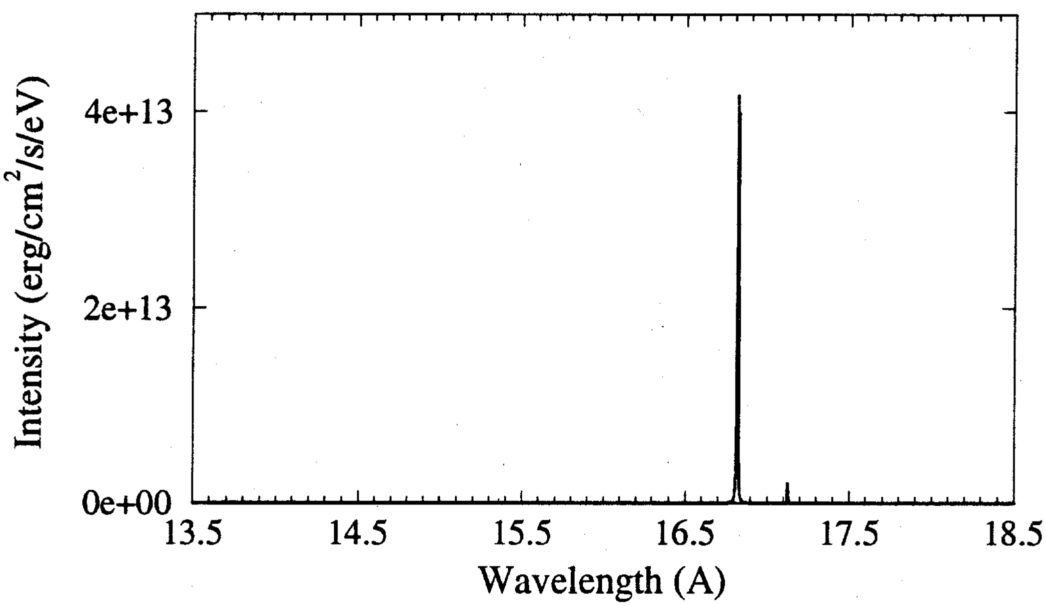

Figure 10(d). Fluorine K_α absorption (top) and emission (bottom) spectra for $T = 20$ eV, $n = 1 \times 10^{18}\,\mathrm{cm}^{-3}$, and $L_o = 1000$ Å. The calculation assumes a 1.0 MeV, 0.3 TW/cm^2 proton beam.